Analytica Chimica Acta 1234 (2022) 340326

Contents lists available at ScienceDirect

Analytica Chimica Acta

journal homepage: www.elsevier.com/locate/aca

Bioanalytical methods encompassing label-free and labeled tuberculosis aptasensors: A review

Onyinyechi Vivian Uhuo *, Tesfaye Taddese Waryo, Samantha Fiona Douman, Kaylin Cleo Januarie, Kelechi Chiemezie Nwambaekwe, Miranda Mengwi Ndipingwi, Precious Ekwere, Emmanuel Iheanyichukwu Iwuoha **

SensorLab (University of the Western Cape Sensor Laboratories), Chemical Sciences Building, University of the Western Cape, Bellville, 7535, Cape Town, South Africa

HIGHLIGHTS

- This review covers TB aptasensors published in the last decade.
- The articles are summarized in terms of years, biomarkers and transduction methods.
- Aptamer sequences and amplification strategies for the aptasensors are discussed.
- The focus is on labeled and label-free aptasensors under different transducers.
- Microfluidic-based TB aptasensors for TB diagnosis were also reviewed.

GRAPHICAL ABSTRACT

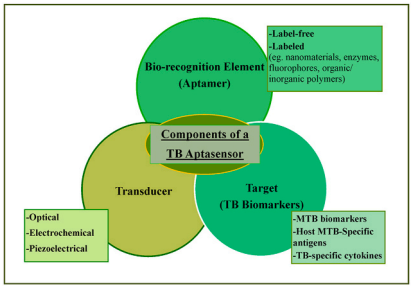

ARTICLE INFO

Keywords:
Tuberculosis
Biosensor
Aptamer sequence
Electrochemical aptasensors
Optical aptasensors
Signal amplification

ABSTRACT

The high incidence of tuberculosis (TB) infection is of great concern world-wide. The traditional TB diagnostic techniques are not ideal for TB diagnosis in resource-poor countries. This is due to their high complexity, expensive nature, long time duration, poor sensitivity and specificity, as well as their requirement for sophisticated laboratories with special biosafety conditions. These limitations are major factors contributing to late diagnosis of TB and its continuous persistence. Biosensors offer several advantages as diagnostic tool due to their independence on *Mycobacterium tuberculosis*, simplicity, low-cost, high sensitivity and specificity. Likewise, the increasing interest on aptamers as biorecognition elements in biosensor application lies in their ease of synthesis and modification, chemical and thermal stability, low-cost, and high sensitivity and specificity towards their targets. Several research works have been done and many more are still on-going on fabrication and application of aptasensors for TB diagnosis. This review summarizes the label-free and label-based electrochemical, piezoelectric and optical aptasensors for TB diagnosis published in the last decade. It focuses on their various aptamer

Abbreviations: TB, Tuberculosis; MTB, *Mycobacterium tuberculosis*; POC, Point-of-care; LTBI, Latent TB infection; IFN-γ, Interferon-gamma; TNF-α, Tumor necrosis factor-alpha; SELEX, Systematic evolution of ligands by exponential enrichment; SAM, Self-assembled monolayer; K_D, Equilibrium binding constant; ECM, Electrochemical; LOD, Limit of detection; LR, linear range; MFS, Microfluidic system.

* Corresponding author.
** Corresponding author.
E-mail addresses: 3824535@myuwc.ac.za (O.V. Uhuo), eiwuoha@uwc.ac.za (E.I. Iwuoha).

https://doi.org/10.1016/j.aca.2022.340326
Received 6 June 2022; Received in revised form 12 August 2022; Accepted 24 August 2022
Available online 30 August 2022

sequence modifications, assay formats, sensitivities, nanomaterial and enzyme-based signal amplification strategies, and the possibility of miniaturization and automation using microfluidic devices.

1. Introduction

Tuberculosis (TB) is a deadly disease of global concern caused by *Mycobacterium tuberculosis* (MTB). Despite numerous efforts to eradicate it, this disease has remained persistent, yearly infecting about 33% of the world population [1]. The World Health Organization (WHO) estimated 9.9 million TB incidence globally in 2020, comprising 56% men, 33% women and 11% children [2]. With an estimated 1.3 million deaths among HIV-negative people (comprising 53% men, 32% women and 16% children) and 214 000 deaths among TB/HIV co-infected patients, TB was the second highest killer from a single infectious agent and of HIV-positive patients in 2020 after COVID-19 [2]. TB infection can be asymptomatic (Latent TB infection, LTBI) or active. Though only about 10% of all TB cases are symptomatic [3], factors such as HIV infection, silicosis, diabetics mellitus, cigarette smoking, malnutrition, overcrowding and poverty may increase the risk of TB infection or activation of LTBI [4]. 68% of the TB cases occur in the WHO African and Asian regions while only 5.3% TB cases occur in the WHO America and European regions [5]. This is largely due to low-economic development, limited access to TB diagnosis and treatment in these areas, and non-ideal point-of-care (POC) application of existing TB diagnostics. In order to end the global TB pandemic, there is urgent need for highly sensitive and selective POC technique for early diagnosis of TB [6].

The individual challenges of the WHO-recommended techniques for TB diagnosis limit their POC application. Culture method is presently the gold test for definite TB diagnosis due to its high specificity and sensitivity. It is a method of growing MTB, a slow-growing bacterium that takes about 2–6 weeks to culture, in solid or liquid culture media. Hence, the culture method is complex and time-consuming, and requires skilled personnel, culture facilities and special biosafety conditions. The sputum smear microscopic method involves microscopic detection of auramine-rhodamine or Ziehl-Neelsen-stained acid-fast bacteria in sputum samples. It offers a rapid, inexpensive and relatively easy method of TB diagnosis. Despite its popularity in low-income countries, this method is relatively insensitive and largely non-specific [7]. The inefficiencies of these methods are because of their dependence on MTB, reliance on sputum samples which are difficult to produce in children and very sick TB patients, low bacteria load often observed in sputum samples even in active TB cases, and the late manifestations of TB symptoms. The non-sputum-based lateral flow urine lipoarabinomannan (LF-LAM) assay (Determine™ TB LAM Ag, Alere, Waltham, MA, USA) is a cheap assay based on quantification of lipoarabinomannan (LAM), a glycolipid of mycobacteria cell wall, excreted in urine by some TB infected patients, by lateral flow assay. Due to its low sensitivity, WHO recommends LF-LAM assay to be used only to assist TB diagnosis in TB/HIV co-infected adult patients with visible TB symptoms, and maximum CD4 count of 100 cells μL^{-1} [7].

Molecular diagnostics for TB are TB diagnostic techniques that detect and measure changes in specific genetic sequences of oligonucleotides as biological markers for TB infection. Molecular testing may involve nucleic acid amplification strategies such as polymerase chain reaction (PCR) and loop-mediated isothermal amplification (LAMP). WHO-recommended TB molecular diagnostic techniques such as the line probe assay (LPA) and the GeneXpert MTB/rifampicin resistant (Xpert MTB/RIF) assay are becoming increasingly popular because of their high specificity, rapidity and ability to also simultaneously detect drug resistant TB strains. LPA takes less than 48 h and is recommended for use only on smear-positive sputum specimens and MTB isolates. The GeneXpert MTB/RIF has a great potential for use in resource poor countries because of its short test duration of 2 h, less biosafety and skill requirement conditions, as well as its high specificity of 99% and sensitivity of 88% similar to that of liquid culture [7]. Its use is still limited due to the high demand for stable power supply and temperature specificity. TB loop-mediated isothermal amplification (TB-LAMP) assay, (Eiken Chemical Company Ltd Tokyo, Japan) is a manual colorimetric assay which requires less than 1 h test duration. It is only recommended as a possible replacement for sputum-smear microscopy for pulmonary TB diagnosis in adults showing TB signs and symptoms [8].

LTBI can be detected using tuberculin skin test (TST) or interferon-gamma release assays (IGRAs). TST is based on immunological response of TB-infection to purified protein derivatives (tuberculin) injected on the skin. The test result is read after 48–72 h as the presence (size and number) or absence of indurations around the injection site [9]. Due to its low specificity, TST gives false-positive results from *nontuberculous mycobacteria* (NTB) infections, prior BCG vaccination, and allergic reaction or hypersensitivity to tuberculin. On the other hand, false-negative TST result may be obtained in children, and as a result of immunosuppression due to 8–10 weeks old TB infection, infectious mononucleosis, steroid use, malnutrition, immunosuppressive treatments, sarcoidosis, live virus vaccine and upper respiratory virus infection. IGRAs are based on monitoring the release of IFN-γ cytokine by IFN-γ secreting T-effector cells when exposed to TB antigens *in vitro*. IGRAs are nonspecific, expensive and require specialized laboratory and skilled personnel. They cannot distinguish active from LTBI [10]. Commercial IGRAs such as QuantiFERON Gold In-Tube assay (QFT-GIT) (Cellestis Limited Carnegie, Victoria, Australia) measures IFN-γ release when exposed to TB antigens by enzyme-linked immunosorbent assay (ELISA), while T.SPOT.TB assay (Oxford immunotech, Oxford UK) measures the number of TB-specific T cells that release IFN-γ on exposure to TB antigens by enzyme-linked immunospot assay (ELISpot). Both QFT-GIT and T.SPOT.TB assays are based on 6-kDa early secretory antigenic protein (ESAT6) and 10-kDa culture filtrate protein (CFP10) [10] TB antigens.

1.1. Biomarkers for TB diagnosis

Over the years, the need to overcome the limitations of the existing techniques has spurred increased research on “ideal” TB diagnostics. This has led to advances in identification and applications of various TB biomarkers [11]. According to Atkinson et al., “biomarkers are characteristics which serve as measurable indicators of normal or pathogenic biological process, or a pharmacological response to a therapeutic intervention or vaccination” [12]. They are used as diagnostic tools [13], as indicators of disease prognosis, as surrogate endpoint, for prediction and monitoring of clinical response to treatment, and measurement of toxicity levels. Biomarkers for TB diagnosis include volatile organic compounds from breath, host MTB-specific antigens, cytokines and chemokines, as well as MTB biomarkers such as the LAM component of MTB cell wall, and the highly conservative repetitive insertion sequence element, 1S6110, of MTB DNA [14,15].

Host MTB-specific antigens such as ESAT6, CFP10, 28-kDa MTB protein (MPT64), 30 –32 kDa antigen 85 complex (Ag85) and heat shock proteins (HSPs). ESAT6 and CFP10 are virulent factors important for growth and pathogenesis of MTB, respectively expressed by the Rv3874 and Rv3875 genes, in the RD1 region of MTB genome during the early stage of MTB growth. MPT64 is expressed by the Rv1980c gene of the RD2 region of MTB genome of actively growing MTB strain. These genes are absent in NTB and BCG vaccine strains [16]. Hence, ESAT6, CFP10 and MPT64 are highly specific for MTB and can distinguish MTB infections from BCG vaccinated population. Ag85 is a secreted antigen for TB diagnosis and treatment, comprising of Ag85A, (Rv3804c, FbPA), Ag85B (Rv1886c, FbPB) and Ag85C (Rv0129c, FbPC). Ag85 complex

possesses enzymatic mycolyl-transferase activity essential for mycobacterial virulence and pathogenesis [17]. These MTB-specific antigens induce proliferation of T cells and cytokine production and release with relation to TB infection. HSPs are also antigenic biomarkers of MTB. They are well conserved intracellular proteins expressed by all cells under stress conditions. They serve as molecular chaperons and their stress-related over-expression allow for microbial survival in host bodies. TB-specific HSPs include host HSP90, HSP70, HSP60 and HSP25, and MTB HSP16 for LTBI [18].

Cytokines are small glycoprotein produced by immune cells to regulate immune response. Common TB-specific cytokines include the pro-inflammatory cytokines such as interferon-gamma (IFN-γ), tumor necrosis factor alpha (TNF-α), interleukin (IL)-12 and IL-18, and the anti-inflammatory cytokine IL-10. TNF-α is mainly expressed in activated macrophages, T cells, monocytes and dendritic cells. It regulates cell apoptosis, and is also involved in immune response during early inflammatory stage by inducing production of other cytokines such as IL-8, C–C Motif Chemokine Ligand 3, and reactive oxygen and nitrogen species. It also upregulates expression of adhesion molecules such as intercellular adhesion molecule 1 by vascular endothelial cells. TNF-α therefore promotes migration and adhesion of immune cells to infected sites, aiding control of disease progression. Elevated levels of TNF-α have been associated with active pulmonary TB infection [19]. IFN-γ is a pleiotropic cytokine which upregulates many cellular functions, including innate and adaptive immune response against pathogen attack, through direct effect on specific gene expression. IFN-γ is produced by $CD4^+$ T helper cell Type 1 (Th1) lymphocytes, $CD8^+$ cytotoxic lymphocytes, natural killer (NK) cells, B cells, natural killer T (NKT) cells as well as professional antigen-presenting cells (APCs) such as monocytes, macrophages and dendritic cells, and can bind to cell surfaces of almost all cell types. IFN-γ promotes immune response against intracellular pathogens and chemically induced tumor. It is a potent macrophage activator which enhances proliferation of Th1 cells, inhibits production of Th2 cells, and induces apoptosis of many cells including tumor cells [20]. Production of IFN-γ by NK cells and APCs is likely important for early host defense against infection while production of IFN-γ by T lymphocytes is important for adaptive immune response during the course of disease. Also, IFN-γ produced by APCs may contribute in locally activating cells and neighboring cells. IFN-γ production is regulated by cytokines and chemokines secreted by APCs. While IL-12, macrophage-inflammatory protein-1α and IL-18 promote IFN-γ production, IL-4, IL-10, transforming growth factor-β and glucocorticoids decrease IFN-γ production in response to pathogen recognition [21]. Over-expression of IFN-γ by T cells and monocytes have been associated with many inflammatory diseases including TB. Also, IL-6 is a cytokine secreted by monocytes, endothelia cells and adipose tissues, which plays important role in acute phase response. Increased level of IL-6 (as well as IL-13 and TNF-α) production has also been observed in activated bronchalveolar cells, especially alveolar macrophages [22], for alveolar inflammation of active TB. IL-6 regulates production of acute phase proteins and immunoglobulin secretion, and promotes B cell maturation and early differentiation of T cells. IL-6 also modulates transition from acute to chronic inflammation by regulating the nature of leucocytes infiltrate, thereby exhibiting proinflammatory profile in models of chronic inflammatory diseases, and anti-inflammatory profile in models of acute inflammation [23,24]. IL-6 has been reported as a positive regulator of IFN-γ release in MTB-infected mice, and as a possible modulator of granuloma formation and control of MTB in humans. Elevated levels of IL-6 is associated with inflammatory and lymphoproliferative disorders and also with TB [25]. IL-2 is a cytokine majorly produced by activated $CD4^+$ and $CD8^+$ T cells, and in some cases by NK, NKT and dendritic cells. It promotes T cell proliferation, B cells and monocytes activation, and cytotoxic T lymphocytes (CTLs) generation [26]. High serum level of IL-2, which reduced with effective anti-TB therapy, was reported in active pulmonary TB patients [27]. IL-2 was also reported as a potential biomarker for differentiating active from LTBI based on its increased production in whole blood after 72 h antigen-stimulation [28].

Chemokines are chemotactic cytokines that regulate and direct movement of leukocytes. IFN-γ inducible-protein-10 (IP-10), also known as C-X-C motif chemokine 10 (CXCL10), is a chemokine of the C-X-C family which regulates migration of Th1 cells. It is a ligand of the CXCR3 receptor and is encoded by the CXCL10 gene. IP-10 is constitutively expressed by stromal cells of lymphoid organs, and also secreted by monocytes, endothelia cells and fibroblasts on stimulation with IFN-γ. *in vitro* expression of IP-10 can also be induced with TNF-α, IL-1α, IL-6, lipopolysaccharide, IFN-α and IFN-β. Functions of IP-10 include chemoattraction of activated T cells, monocytes and NK cells to inflammation sites during adaptive immune response; promotion of T cell adhesion to endothelia cells; anti-tumor activity; and inhibition of endothelia cell production. IP-10 has been described also as a modulator of other antitumor cytokines. High level of IP-10 has been associated with Th1-type inflammatory diseases and auto-immune diseases [29]. Elevated levels of IP-10 have also been observed in serum of active and latent TB infected patients [13].

Biosensing techniques for TB-biomarkers include immunoassay techniques (such as ELISA and ELISpot), and biosensor technique. Though immunoassays are sensitive and cost-effective, they require multiple separation and washing steps, and hence are labor intensive and time consuming. Example of commercial immunoassay for TB biomarker is the IGRAs.

1.2. Biosensor approach to TB-biomarker detection

A biosensor is an analytical device which measures biological targets based on biochemical reaction between the target and biorecognition element, and converts the biochemical response into measurable signal using a biotransducer element and electronic system [30]. Unlike immunoassays and other bioanalytical devices, biosensors require no additional processing steps and can be repeatedly calibrated. They offer a simple, rapid, cost-effective, highly sensitive and specific method of detecting biomarkers, with possibility of miniaturization, automation and POC application. Biosensors may be classified based on the biorecognition element, mechanism of interaction, or based on the biotransducer. For TB biosensor fabrication, antibodies [31,32], nucleic acids [33–35], engineered protein [36], affinity binding receptors [37], enzymes and aptamers [38] have been explored as biorecognition elements. The increasing interest in the use of aptamers as recognition element, compared to enzymes and antibodies, lies in their high affinity and specificity to targets in the nanomolar to picomolar range, and high chemical stability within pH range of 2–12. Aptamers also have high resistance to enzyme activities, low-to-no immunogenicity, and high thermal stability with a certain degree of thermal refolding. Aptamer selection process (SELEX) are faster, simpler and cheaper, and can be realized *in-vitro* and *in-vivo* with ease of chemical modifications. The different components of an aptamer-based biosensor (aptasensor) is illustrated in Fig. 1.

Over the years, several review articles relating to biomarker-based TB diagnosis have been published. While the focus of some of the articles was too broad such that very little attention was paid to aptasensor-based TB diagnosis [39–41], in some others, the focus was quite narrow covering only IFN-γ [42,43], electrochemical transduction [44] or label-free nano-biosensors [45]. Hence, in this review, we summarized the electrical (electrochemical and piezoelectrical) and optical-based aptasensors for TB diagnosis with focus on aptamer sequences and modifications, assay formats, signal amplification strategies, and analytical performance of the TB aptasensors. Unlike in the article published by Golichenari et al. (2018) on "Nano-biosensing approaches on tuberculosis: defy of aptamers", where the aptasensors were discussed based on the class of target protein (whole cells of M. tuberculosis, mycobacterial proteins and IFN-γ), in this review, we classified the aptasensors based on label-free and label-based aptasensors with

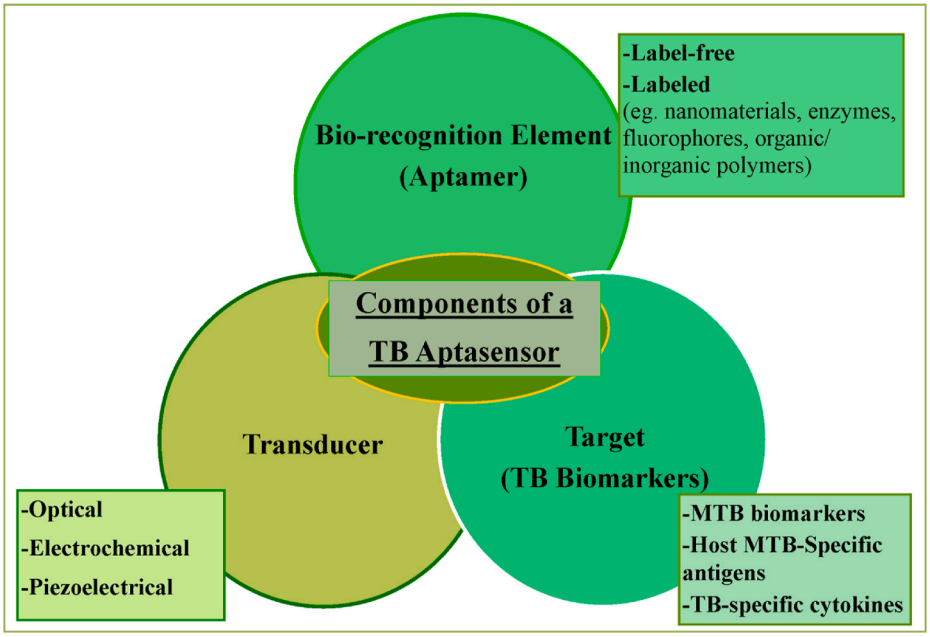

Fig. 1. Components of a TB aptasensor.

emphasis on the methods of signal amplifications using nanomaterials, enzyme-assisted target recycling and amplification techniques. A total of 61 publications (comprising 64% electrical and 36% optical) were reviewed. Summary of these articles (Figs. 2 and 3) in terms of number of publications per year, biomarker type, electrical and optical-based techniques, show that there is a noticeable increase in published

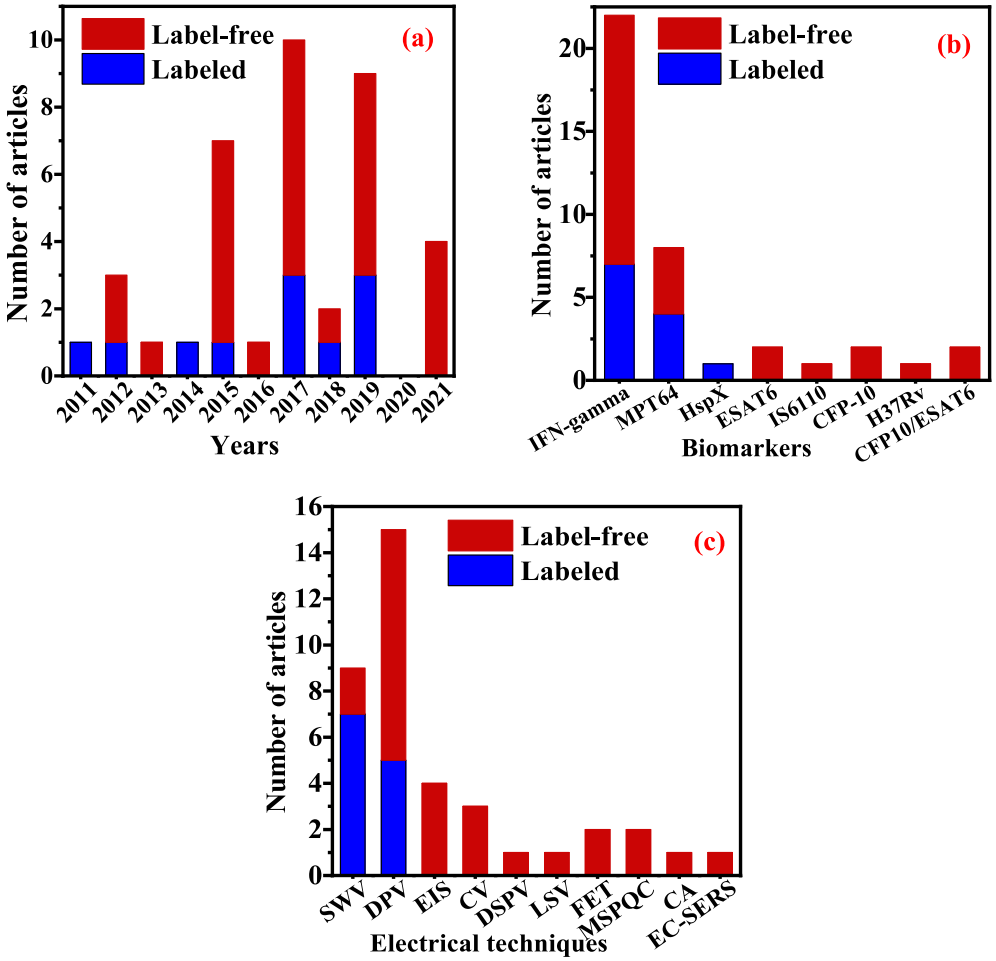

Fig. 2. Summary of electrical based TB aptasensors based on the number of publications per year (a), biomarker type (b) and detection techniques (c).

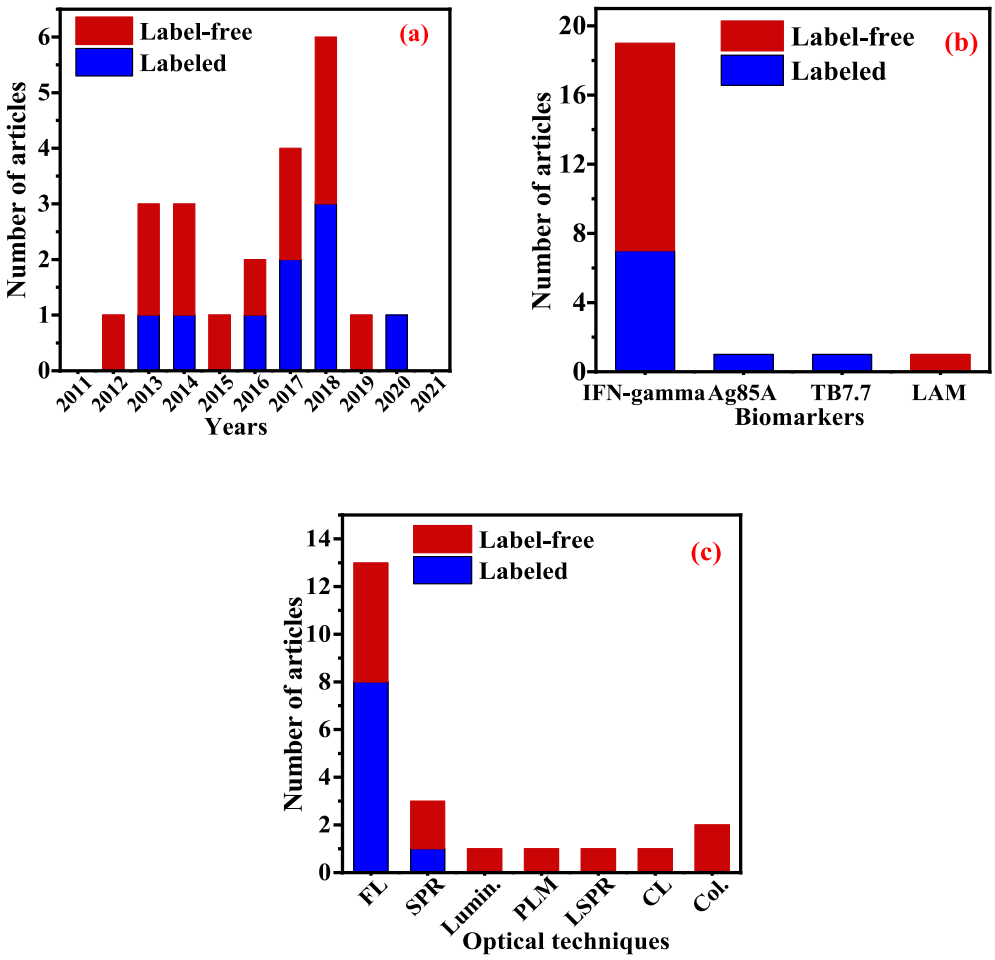

Fig. 3. Summary of optical aptasensors reviewed, based on the number of publications per year (a), biomarker type (b) and detection techniques (c).

articles on TB aptasensors since the last decade. Also, IFN-γ is the most widely studied biomarker for TB aptasensors, accounting for 67% of all the articles review (56% of all electrical, and 86% of all optical based aptasensors). Label-free aptasensors accounted for 69% and 59% of all electrical and optical aptasensors under review, respectively, and were majorly detected using Differential Pulse Voltammetry (DPV), Squarewave Voltammetry (SWV), fluorescence (FL) and Surface Plasmon Resonance (SPR) techniques.

1.3. Aptamer sequence, structure and modifications for TB aptasensors

Aptamers are single stranded oligonucleotides capable of folding and binding to target molecules with high selectivity and specificity. These aptamer molecules are selected *in vitro* by a technique known as systematic evolution of ligands by exponential enrichment (SELEX) from a very large random DNA libraries (or RNA library transcribed from DNA library) [46], of about 10^{13} to 10^{15} variants. The SELEX technique involves the following steps: incubation of the oligonucleotide library with target molecule at appropriate conditions; binding of the oligonucleotide to target molecule; removal of unbound target; splitting of target/oligonucleotide complexes; PCR sequence amplification and purification, and characterization of selected oligonucleotide (aptamer) [47]. Though very effective, the conventional SELEX requires about 15–20 selection rounds and may take up to a month [48]. The need to reduce the time and labor requirement, has led to continuous modification of the conventional SELEX. Capillary electrophoresis-SELEX employs differences in electrophoretic mobility to separate the aptamer-target complex from the unbound oligonucleotide in days, after four selection rounds [49]. Magnetic beads SELEX ensures ease of miniaturization and possibility of automation [50]. Whole cell SELEX can generate high affinity aptamer for whole live cell without prior knowledge of the target [51]. In order to overcome the challenge of loss of activity of *in vitro* SELEX aptamers when applied *in vivo,* aptamers can be generated via *in vivo* SELEX directly within living cells [48]. SELEX techniques, in combination with microfluidic systems, can ensure rapid and efficient aptamer selection at reduced cost [52].

Both RNA and DNA aptamers has been reported for TB biomarkers (Tables 1 and 2). The choice of aptamer sequence is crucial in aptasensor fabrication. This is because the particular aptamer sequence determines to a large extent the mechanism of interaction of the aptamer to the target analyte and the mode of detection of the aptasensor. Hence, modifications to existing aptamer sequence may be made for specific purposes. For instance, the most common functional sequence contained in most IFN-γ aptamer sequence is a guanine (G)-rich sequence, 5′-GGGGTTGGTTGTGTTGGGTGTTGTGT-3′, capable of folding into stable G-quadruplex (G-quad) secondary structure in the presence of cations. Effect of spacers and modifiers on the equilibrium binding affinity of this aptamer sequence to IFN-γ showed equilibrium binding constant (K_D) of 3–28 nM, with 3′-biotintylated modifier having the lowest K_D and thus the highest affinity to IFN-γ [53]. Formation of high affinity IFN-γ hairpin aptamer structure was made possible by extension of the 3′ terminus by -CCAACCCC- sequence for the self-hybridization of the 5′-GGGGTTGG- with the 3′-CCAACCCC- sequence. This gave a K_D of $3.4 \pm 0.47 \times 10^{-10}$ and $3.11 \pm 0.84 \times 10^{-10}$ with and without conjugation to methylene-blue (MB) redox tag [54]. Other modifications include addition of complementary sequence for hybridization chain reaction (HCR), addition of DNAzyme sequence for the formation of peroxidase

Table 1
Aptamer sequence for electrochemical TB aptasensors.

Target	Aptamer/electrode interaction	Label	Aptamer sequence (5′-3′) with references	Post-SELEX modification (equilibrium binding constant, K_D, in nM)
BoIFN-γ	Au–S SAM	5′-MB	NH_2–C6-TTGCCCAACGTGGTGTTTATCACCTTGGATTC-C3-SH [60]	- MB conjugation (K_D NR)
IFN-γ	Au–S SAM	5′-MB	NH_2–C6-GGGGTTGGTTGTGTTGGGTGTTGTGTCCAACCCCC3-SH [54]	-MB conjugation; (from $3.11 \pm 0.84 \times 10^{-1}$ to $3.40 \pm 0.47 \times 10^{-1}$)
	Au–S SAM	5′-MB [61–64] 5′-AQ [65]	NH_2–C6-GGGGTTGGTTGTGTTGGGTGTTGTGTCCAACCCCC3-SH [61–65]	- MB conjugation (K_D NR) [61–64] -AQ conjugation (K_D NR) [65]
	Streptavidin-A-DDAH	–	GGGGTTGGTTGTGTTGGGTGTTGTGTACTATAGGATTGACCGCTGTGTGACGCAACACTCAATAAAAAAAAAA [55]	-AuNPs bioconjugation (K_D NR)
	Au–S SAM	–	CTCTCTGGGGTTGGTTGTGTTGGGTGTTGTGTTCTCTC [58]	-NA (K_D NR)
	Hybridization	–	GGGGTTGGTTGTGTTGGGTGTTGTGTCCAACCCC [66]	-NA (K_D NR)
	Au–S SAM	–	RNA Aptamer: HS–$(CH_2)_{12}$–GGGAGGACGAUGCGGACACCGUU-AAUCUGAGGCCCUGUCCUAUUCCUUCACGCCUCAGA [67,68]; DNA Aptamer: HS–$(CH_2)_{12}$–GGGGTTGGTTGTGTTGGGTGTTGTGT [67]	-NA (K_D of RNA 18.7 ± 1.2 K_D of DNA 63.8 ± 7.4)
	Hybridization	–	SH-CCCCAATCCAGGGGTTGGTTGTGTTGGGTGTTGTGTCCCC-TGGATTACACAA [69]	-NA (K_D NR)
	Au–S SAM	–	CCCTGGGCTCAACCTAGGAATCGCGTTGGTTGTGTTGGG-TGTTGTGTGCGATTCCT-SH [70]	-NA (K_D NR)
	Au–S SAM	–	GGGGTTGGTTGTGTTGGGTGTTGTGTCCAACCCC-C6-SH [71]	-NA (K_D NR)
	π-π interaction		/Pyrene/GGGGTTGGTTGTGTTGGGTGTTGTGT [72]	-NA (K_D NR)
	Au–S SAM [74] Hybridization [57]	–	AAAGGGGTTGGTTGTGTTGGGTGTTGTGTCCAACCCC [57,73]	-NA (K_D NR)
	π-π interaction	–	GGGGTTGGTTGTGTTGGGTGTTGTGT [74]	-NA (K_D NR)
	Au–S SAM	–	SH–$(CH_2)_6$- GGTCTCAGTCAGGGGGTTGGTTGTGTTGGGTGTTGTG-TCTGACTG [75]	-NA (K_D NR)
	Au–S SAM	–	CCCTGGGCTCAACCTAGGAATCGCTTTTTTGGGGTTGGTTGTGTTGGGTGTTGTGT [76]	-NA (K_D NR)
	Au–S SAM	–	GGGGTTGGTTGTGTTGGGTGTTGTGTGGGTAGGGCGGGTTGGGCCAACCCC-C3-SH [77]	-NA (K_D NR)
	Au–S SAM		CCGCCCAAATCCCTAAGAGAAGACTGTAATGACATCAAACCAGACACACTACACACGCATTGC-CATGTGTATGTGGG [78]	-NA (K_D NR)
MPT64	-Au-S -SAM [79–81] -π-π interaction [82]	-Au-C_{60}NPs -N-CNTs/GO [79] -Au@PB -HRP [80] -AuNPs-MOF [81] -GNPs-C_{60}-PAn [82]	SH–$(CH_2)_6$-TGGGAGCTGATGTCGCATGGGTTTTGATCACATGA SH–$(CH_2)_6$-TTCGGGAATGATTATCAAATTTATGCCCTCTGAT [79–82]	-NA (K_D NR)
	Au–S SAM		HS-(CH_6)6-OP(O)2O-(CH_2CH_2O)6-5′-TTTTT-aptamer [83,84]	-NA (K_D of 8.92)
	Biotin-Streptavidin	–	[Btn]-GTACAAACGACGGCCAGTCCTTGGGATGATTCAAGCAAA-GCCTCACGCCTACGGCTAAGTCATAGCTGTCTCTCCTG [85,86]	-NA (K_D NR)
HspX	Au–S SAM	5′-MB	AGGGCTTTTTTTTTTTTTTAGTTCGTTTG-C6-SH [87]	-MB conjugation (K_D NR)
CFP10-ESAT6	Hybridization	–	GGGAGCTCAGAATAAACGCTCAAACGTATTCCATAGTGCTTTATTACTCGCACTTGTGTTCGACATGAGGCCCGGATC-C6 [88] NH_2-GCCTGTTGTGAGCCTCCTAACCCCATCTTATACGTATATGG-ACTCATCTCGACCCCCGATAGGCTTGGTACATGCTTATTCTTGTCTCCC [89]	-NA (K_D NR)
CFP10	Hybridization		CCTGAAAGGGGCCTGCCCCACTATCTCACATGGGGTTCAGTTGGTTGTACG [90]	-NA (K_D NR)
ESAT6	Au–S SAM	–	SH–$(CH_2)_6$–GGGAGCTCAGAATAAACGCTCAACCTCCCTGGGTCAC-CATAGACTCCATCTAAGATGCTTCGACATGAGGCCCGGATC [91]	-NA (K_D NR)
	PO_4^{3-}-Zr^{4+}		PO_4^{3+}-GGGAGCTCAGAATAAACGCTCAACCTC CCTGGGTCACCA-TAGACTCCATCT AAG ATGCTTCGACATGAGGCCCGGATC [92]	-NA (K_D NR)
H37Rv	Au–S SAM	–	SH-GGGAGCTCAGAATAAACGCTCAACCCTGCGGGGCTGCCCGA-TATGT-GTCCAAGTGGTGTTCGACATGAGGCCCGGATC [93]	-NA ($K_D = 37 \pm 4$)
IS6110	Ag–S SAM		/5ThioMC6-D/TCCTGGGCTGGCGGGTCGCTTCC [94]	-NA (K_D NR)

Table 2
Aptamer sequence for TB optical aptasensors.

Target	Labels	5′-3′	Technique/ref.	Post-SELEX modification (equilibrium binding constant, $K_{D,}$ in nM)
IFN-γ	FAM	Biotin-GGGGTTGGTTGTGTTGGGTGTTGTGT (5′B), GGGGTTGGTTGTGTTGGGTGTTGTGT-Biotin (3′B) Biotin-C12-GGGGTTGGTTGTGTTGGGTGTTGTGT (5′B_{spacer}) GGGGTTGGTTGTGTTGGGTGTTGTGT-C12-Biotin (3′B_{spacer}) 6-FAM-GGGGTTGGTTGTGTTGGGTGTTGTGT-Biotin (FA)	SPR [53]	Effect of position of attachment via avidin-biotin interaction and spacers (28.1 ± 1.09 for 5′B; 3.44 ± 0.2 for 3′B; 14.9 ± 1.3 for 5′B_{spacer}, 6.56 ± 0.8 for 3′B_{spacer}, and 5.73 ± 1.1 for FA)
	TPE	NH_2–C6-GGGGTTGGTTGTGTTGGGTGTTGTGT	FL [95]	TPE conjugation (K_D NR)
	BODIPY, Fluorescein, TAMRA, Alexa Fluor	TGTTAGGGGGTTGGTTTTGGGTTGG	FL [96]	Label conjugation (K_D of123.6 ± 14.6 nM with BODIPY-label and 33.7 nM with fluorescein-label
	GQDs	NH_2–C6-GGGGTTGGTTGTGTTGGGTGTTGTGT	FL [97]	GQDs conjugation (K_D NR)
	FAM	TAGTATACGGAGTGGGGTTGGTTGTGTTGGGTGTTGTGTTTTTTTTACACAACAC	FL [98]	FAM labeling (K_D NR)
	FAM	GGGGTTGGTTGTGTTGGGTGTTGTGT	FL [99]	FAM labeling (K_D NR)
	3′ Chol; 5′-ROXN	/ROXN/AGGGGTTGGTTGTGTTGGGTGTTGTGTCCAACCCCT/TAO//iSp18//3CholTEG/	FL [100]	Chol. and ROXN labeling (K_D NR)
	FAM	6-FAM-TGGGGTTGGTTGTGTTGGGTGTTGTGT	FL [101]	FAM labeling (K_D NR)
	–	TGGGGTTGGTTGTGTTGGGTGTTGTGT	FL [102]	-NA (K_D NR)
	–	GGGGTTGGTTGTGTTGGGTGTTGTGT	FL [103], Col [104].	-NA (K_D NR)
		GGGGTTGGTTGTGTTGGGTGTTGTGT-biotin	CL [105]	-NA (K_D NR)
	–	HS-GGGGTTGGTTGTGTTGGGTGTTGTGTATTGACCGCTGTGTGAC-GCAACACTCAAT HS-GGGGTTGGTTGTGTTGGGTGTTGTG TTTTTTTATTGACCGCTG-TGTGACGCAACACTCAAT HS-GGGGTTGGTTGTGTTGGGTGTTGTGTTTTTTTTTTTTTTTATTG-ACCGCT-GTGT GACGCAACACTCAAT	SPR [56]	-NA (K_D NR)
	–	AACTTCACTAGGGGTTGGTTGTGTTGGGTGTTGTGTCCCCTAGTGAAGTT	FL [106]	-NA (K_D NR)
	–	NH_2–C6-GGGGTTGGTTGTGTTGGGTGTTGTGT	PLM [107]	-NA (K_D NR)
	–	TGGGGTTGGTTGTGTTGGGTGTTGTGT-C3-thiol	LSPR [108]	-NA (K_D NR)
	–	NH_2–C12-AAAAAAAATCCAGGGGTTGGTTGTGTTGGGTGTTGTGT-CCCCTGGAT TACACAA	FL [109]	-NA (K_D NR)
	–	Biotin-CCAAAAAAAAAAAAAAAAAAAAAAAGGGGTTGGTTGTGTT-GGGTGTTGTG TATTTTTTTTTTTTTTTTTTTTT	FL [110]	-NA (K_D NR)
	–	GGGGTTGGTTGTGTTGGGTGTTGTGTTTTTTTTTTTTTTATTGACCGCTGTGTGAC GCAACACTCAAT	SPR [111]	-NA (K_D NR)
Ag85A (FbPa)	ATTO647N	GCTGTGTGACTCCTGCAAGCGGGAAGAGGGTAAGGGGAGGGAGGGTAACGCGGA GAAGGCAAGCAGCTGTATCTTGTCTCC (Apt 22) GCTGTGTGACTCCTGCAATCAGGAAAGAACTTAGGGGTGGGAGGAGGGTATAAATA CGGAATG-CAGCTGTATCTTGTCTCC (Apt 8)	FL [112]	-ATTO647 N labelling (K_D of 62.95 and 202 for ATTO647N-Apt22 and ATTO647N-Apt8
TB7.7	FAM, BHQ1	CACCTAATACGACTCACTATAGCGGATCCGA	FL [113]	-FAM and BHQ1 conjugation (K_D = 5.3)
LAM	–	GGCGCCATAGCGACGGGGCCATTCCAAGAA-biotin (direct dot-blot) GCGGAATTCTAATACGACTCACTATAGGGAACAGTCCGAGCCGGCGCCATAGCGACGG GGCCATTCCAAGAAGGGTCAATGCGTCATA (indirect dot-blot assay)	Col [114].	-NA (K_D NR)

mimicking G-quad DNAzyme [55], addition of streptavidin sequence for hybridization with streptavidin reporter molecule [56], addition of -AAA- to the 5′ terminal for exonuclease digestion [57], and extension of the 5′ and 3′ terminal by -TCTCTC- for the formation of triple-helix molecular switch system [58].

The aptamer sequence terminals may be modified for immobilization on solid surfaces, or conjugation to labels and oligonucleotides. Conjugation is achieved through interaction between the modified terminal moiety of the aptamer and the functional groups of the dye, complementary oligonucleotide or the solid surface. Aptamer molecules may be directly labeled with dyes or terminated with functional groups (such as $–NH_2$-) for conjugation with dyes. Aptamer labels mostly serve as redox probes/reporter molecules, and as signal amplifiers. Common aptamer labels include enzymes, organic and inorganic dyes, and nanoparticles. Aptamers may be immobilized on transducer surfaces with either the 5′ or the 3′ end by physisorption, chemisorption, covalent attachment and streptavidin-biotin interaction [59]. The physisorption method involves physical adsorption of aptamers on electrode surfaces as a result of electrostatic interaction between them. This process is simple and does not require modification of the nucleic acid terminals of aptamers, but it is prone to aptamer desorption from electrode surface and therefore not suitable for fabrication of reusable aptasensors [59]. Aptamers with thiolated 5′ or 3′ end can be chemically adsorbed onto gold electrodes by chemisorption method. This is due to the strong affinity of Au for S, forming self-assembled monolayer (SAM) of Au–S on the electrode surface. Aptamers terminated with reactive functional groups can form chemical bonds with reactive electrode surfaces via covalent attachment. In some cases, this can be achieved using crosslinkers such as 1-ethyl-3-(3-dimethylaminopropyl) carbodiimide/N-(2-hydroxyethyl) succinimide (EDC/NHS) for immobilization of $–NH_2$-terminated aptamer on –COOH functionalized graphene [97]. Likewise, biotin terminated aptamers can be immobilized on streptavidin modified substrates due to the strong interaction between biotin and streptavidin. Aptamers can also be indirectly immobilized on substrate surfaces by hybridization with complementary oligonucleotides possessing functionalized sequence terminals via the strong affinity of the modified terminal moiety of the complementary oligonucleotide to the substrate surface [59].

1.4. Transduction methods and the need for signal amplification

Aptasensor transduction methods are the various methods of converting biochemical response resulting from aptamer-target interactions into measurable signals which are proportional to the concentration of the target analyte. Different transduction methods are capable of recognizing this response as different forms of changes in the system, and transforming these changes into measurable electrochemical, optical, mass or magnetic signals. Some of the individual challenges of different transduction methods include low sensitivities of colorimetric techniques, high cost of fluorescence and surface plasmon resonance techniques, heterogeneity of electrochemical probe surfaces and the interaction between probe and recognition element/target. These limitations coupled with the need for miniaturization and improved technological efficiency have led to great advancement in the area of signal amplification. Methods of signal amplifications reported for TB aptasensors include the use of conductive materials such as polymers, organic and inorganic materials, and nanomaterials, either as sensing platforms or as aptamer labels. Likewise, nucleic acid amplification techniques such as polymerase chain reaction (PCR) [15], loop-mediated isothermal amplification (LAMP) [106], hybridization chain reaction (HCR) [70,115], as well as enzyme-assisted target recycling (EATR) [116] techniques have also been applied for target recycling and signal amplification of TB biosensors.

2. Electrochemical TB aptasensors

Electrochemical aptasensors are aptasensors that detect and measure changes in electrochemical properties resulting from aptamer-target interaction. In this type of aptasensors, target-specific aptamers are immobilized on electrode surfaces which serve as the transducer. Detection is achieved as a result of the high affinity of aptamers to their target molecules, forming aptamer/target duplexes. This results to increase (“signal on” or “turn-on”) or decrease (“signal off” or “turn-off”) in electrochemical signals. Based on the specific aptamer sequence and the mechanism of aptamer/target interaction, target binding leads to specific changes such as conformational change in aptamer hairpin or G-quad structures, dissociation of dsDNA formed by aptamers and other oligonucleotides, dissociation of sandwich systems, or change in charge transfer impedance, upon target binding. Depending on the electrochemical quantity being measured, electrochemical aptasensors are broadly divided into: potentiometric (changes in potential difference), amperometric/voltammetric (changes in current at fixed/varied potential), impedimetric (changes in resistance and capacitance) and conductometric (changes in solution conductance) techniques. Cyclic voltammetry (CV), squarewave voltammetry (SWV), linear sweep voltammetry (LSV), differential pulse voltammetry (DPV), differential stripping pulse voltammetry (DSPV), chronoamperometry (CA), chronocoulometry (CC), electrochemical impedance spectroscopy (EIS), and source-drain current measurements of field effect transistors (FET) have been extensively reported for characterization and application of electrochemical aptasensors. Compared to optical, magnetic and piezoelectric transduction methods, electrochemical transduction offers higher sensitivity, simplicity, portability, low cost, and minimal power requirement. Design of TB aptasensors under this review is classified based on the use of label-free or labeled aptamer recognition molecules.

2.1. Label-based TB electrochemical aptasensors

Label-based TB electrochemical aptasensors use aptamer molecules labeled with redox compounds such as fluorophores, nanomaterials, or enzymes as recognition elements (Table 3). Aptamer labels, while serving as redox probes for biomarker detection, may also increase the signal-to-noise ratio. Target detection using label-based TB aptamers are based on different assay formats. For instance, detection using labeled hairpin aptamers is based on conformational change in the aptamer hairpin structure upon target binding. In the absence of target, labeled-hairpin aptamers when immobilized on electrode surfaces form stable hairpin structures with the label close to the surface. In the presence of target, switching of the hairpin structure and formation of aptamer/target duplex displaces the label from the surface, leading to reduction in electrode transfer efficiency and “Signal-off” format. Using this assay format, with methylene blue (MB)-labeled aptamers immobilized on gold disk electrodes (GDE), limit of detection (LOD) of 0.1 nM has been reported for BoIFN-γ aptasensor [60] and 0.06 nM for IFN-γ aptasensor [54]. In a similar report, an IFN-γ aptasensor with LOD of 1.3 ng mL^{-1} offered a better opportunity for future POC application by incorporating Au microelectrode technology (Fig. 4) [63].

2.1.1. Nanomaterial-assisted label-based electrochemical TB aptasensors

For improved aptasensor performance, nanomaterials have been employed either as aptamer labels or as sensing platforms in label-based TB aptasensor design. The increasing interest in the application of nanomaterials for biosensor and bioimaging purposes lie in their extremely small sizes, large surface-to-volume ratios, enhanced mechanical, optical and electrical properties, as well as chemical reactivity and conductivity. For instance, using both Au-coated silicon nanowires (SiNWs) and planar Au electrodes as platforms for immobilization of MB-labeled IFN-γ hairpin aptamer, the release of IFN-γ from primary human leukocytes has been reported [62]. When compared to planar Au electrode surface, SiNWs reportedly decreased response time by 3.18

and increased sensitivity by 3.90, with LOD of 150 T cells mL^{-1}. Au nanoparticles (AuNPs) is one of the most extensively studied nanomaterial for immobilization of biomolecules due to its strong affinity for sulfhydryl group. AuNPs, electrodeposited on the surface of screen-printed carbon electrode (SPCE) was used as the sensing platform for a recent HspX TB meningitis aptasensor [87]. "Signal-off" detection, with LOD of 10 pg mL^{-1}, was recorded as a result of structure switching of the MB-labeled HspX hairpin aptamer.

Nanomaterials have also been reported as aptamer labels in sandwich assay format. This sensitive and selective assay format presents a detection format for targets possessing two independent binding sites for binding two ligands (aptamers and/or antibodies) [59] which may or may not be labeled with the same molecule. Detection is monitored as displacement of the tracer label on aptamer/target binding. MPT64 TB biomarker has two independent binding sites, and hence a suitable TB biomarker for sandwich assay format. An MPT64 sandwich aptasensor with a low LOD of 0.33 fg mL^{-1} was recently fabricated with the aptamer probe immobilized on a Au–Pt core-shell nanoparticles (Au@Pt)-modified GCE and polyethyleneimine functionalized iron-based metal organic frameworks (PEI-Fe-MOF). The tracer label contains a different MPT64 aptamer, labeled with AuNPs, fullerene nanoparticles, nitrogen-doped carbon nanotubes and graphene oxide (Au–C_{60}NPs-N-CNTs/GO) nanocomposite. Signal was generated by reaction of the C_{60} with tetraoctylammonium bromide (TOAB) [79]. Bai et al. (2017) reported similar sandwich format for an MPT64 electrochemical aptasensor, with 20 fg mL^{-1} LOD. An MPT64 capture aptamer probe was directly immobilized on Au electrode surface, and another as tracer label (labeled with AuNPs-decorated fullerene (C_{60})-doped polyaniline (GNPs-C_{60}-PAn) nanohybrids) [82]. In a similar study, Li et al. (2019) achieved LOD of 21 fg mL^{-1} with a tracer label containing MPT64 aptamer and horseradish peroxidase (HRP) tagged with AuNPs linked prussian blue nanoparticles (Au@PB-HRP) in the presence of poly (diallyl dimethyl ammonium chloride) (PDDA) [80].

In another sandwich assay based MPT64 aptasensor with 10 fg mL^{-1} LOD [81], two different MPT64 aptamers were simultaneously conjugated alongside HRP, to AuNPs/Zr(IV) metal organic framework (AuNPs/MOF), to form the signal probe. The aptamers were also simultaneously immobilized on Au electrode to serve as the detection probe.

2.2. Label-free electrochemical TB aptasensors

Unlike label-based aptasensors, label-free aptasensors use non-labeled aptamers as recognition element (Table 4). Detection using label-free aptamers is achieved via different mechanisms. For instance, a recently reported IFN-γ aptasensor based on three-way multifunctional label-free aptamer, containing target recognition region, anchoring region and a 4C–C mismatch region for intercalation of Ag^{+} reporter molecule, gave LOD of 0.67 pg mL^{-1} and 0.42 pg mL^{-1} in standard and clinical IFN-γ samples, respectively. Detection was based on the dissociation of the multifunctional aptamer structure on target binding, resulting in release of the Ag^{+} probe and increased signal [78]. A recent label-free "turn-off" aptasensor with LOD of 3 pg mL^{-1} was based on dissociation of triple-helix molecular switch (THMS) system on target binding, resulting to decreased electrochemical recognition of intercalated MB redox probe [58]. THMS system was formed using label-free IFN-γ aptamer with 5′ and 3′ ends extended by a -TCTCTC- sequence, and a signal transduction probe. In another assay format, using label-free aptamers and labeled-complementary DNA/RNA sequences, a multiplex aptasensor for IFN-γ (LOD of 1.14 pM) and lysosome (LOD of 0.0164 nM) was reported. The label-free IFN-γ and lysozyme (Lys) aptamers were partially hybridized with 5′ thiolated ferrocene-labeled IFN-γ signal probe (Fc–IFN–γ SP) and MB-labeled hairpin Lys signal probe (MB-Lys SP), respectively, on the same GDE (Fig. 5) [66]. Target binding induced switching of the hybrid structures, with the Fc label displaced far from the electrode in the presence of IFN-γ ("signal-off"), and the MB label closer to the electrode surface in the presence of Lys ("signal-on").

Label-free aptamers have also been reported for impedance-based TB aptasensors. Detection is based on the degree of hindrance of electron transfer on target binding. Formation of aptamer/target complex decreases electron transfer due to the non-conductivity of target and the negative phosphate backbone of aptamer, resulting in increase in charge transfer resistance, and measured by EIS. Such impedance-based assay strategy was reported for a 20.22 pM LOD EIS-based aptasensor for IFN-γ using AuIDE electrode and an RNA aptamer [68]. Sypabekova et al. (2019) likewise reported an aptasensor for MPT64 protein using similar assay, achieving LOD of 81 fM in spiked human serum with AuIDE electrode as sensing platform [83], and 4.1 fM in buffer with Au disk electrode [84].

2.2.1. Nanomaterials for signal amplification of label-free electrochemical TB aptasensor

Exploring the many advantages of nanomaterials, several label-free aptasensors incorporating nanomaterials as sensing platforms and/or as label molecules have been reported for TB biomarkers. Signal enhancement may be obtained solely with nanomaterials, or in conjunction with other signal amplifiers such as conductive materials (polymers, organic and inorganic materials), enzymes and/or nucleic acid amplification steps. Nanomaterials have been reported, in combination with label-free structure switching hairpin recognition probes for "signal-on" TB aptasensors. In one report by Xu et al. (2019), IFN-γ aptasensor with LOD of 19 fg mL^{-1} used label-free diblock dual-aptamer allosteric hairpin (DDAH), and a nanohybrid sensing platform comprising of streptavidin-$Cu_3(PO_4)_2$ hybrid nanoflower and graphene (SA-$Cu_3(PO_4)_2$HNA-G) (SFG). The structure of the DDAH which also contained polyadenine, streptavidin-binding aptamer and DNAzyme-substrate sequences was switched due to the formation of Mg^{2+}-dependent DNAzyme in the presence of IFN-γ, leading to activation of streptavidin-aptamer complex (Fig. 6) [55]. Similarly, an IFN-γ aptasensor with LOD of 0.57 pM was fabricated using (+)AgNPs redox tags adsorbed on DNA concatemers [69]. Target binding induced switching of aptamer hairpin structure initiating HCR with cycles of DNA hairpin self-assembly.

Likewise, LOD of 16.3 fM was reported by Miao et al. (2017) with nafion (Nf) and (+)AuNPs composite membrane-modified electrode. This aptasensor was based on target-induced switching of capture probe stem-loop structure, which initiates series of HCR of the aptamer stem strand with oligonucleotides, coupled with the strong interaction of iridium(III) complex to the hybrid dsDNA to achieve signal amplification [70]. Jin et al. also fabricated a "turn-on" label-free aptasensor for IFN-γ with LOD of 2 fg mL^{-1} [71], based on target induced switching of aptamer structure, using AuNPs electrodeposited on a poly(amidoamine) (PAMAM) dendrimer matrix/MoS_2 modified GCE sensing platform, and MB adsorbed on the aptamer hairpin as redox probe. Also, signal amplification of a "turn-off" ESAT6 aptasensor with LOD of 0.33 fg mL^{-1} was achieved using GCE modified with a nanocomposite. The nanocomposite comprises of reduced graphene oxide doped with metal-organic framework and functionalized with poly (diallyldimethylammonium chloride) (P-MOF-rGO) for increased loading of electroactive toluidine blue (Tb) reporter probe, and platinum@gold (Pt@Au) nanoparticles sensing platform [91]. A similar "turn-off" ESAT6 aptasensor with LOD of 12 fg mL^{-1} was reported using nitrogen-doped graphene-decorated bimetallic organic framework of Zr-MOF on Ce-MOF as a matrix for loading Tb reporter [92]. In contrast, "turn-on" aptasensing of ESAT6 to 1.5 ng mL^{-1} LOD was achieved using aptamer-antibody sandwich assay format with graphene-polyaniline (GP/PANI)-modified SPCE, label-free aptamer and Fe_3O_4/Au MNPs conjugated antibody probes [89]. In another study, a label-free "signal-on" impedimetric MPT64 TB aptasensor using PEDOT-CNT modified FTO electrode sensing platform was reported with LOD of 0.5 ± 0.2 fg mL^{-1} [85]. Likewise, an MPT64 electrochemical aptasensor, achieved

Table 3
Label-based electrochemical aptasensors for TB biomarkers.

Target	Electrode/ immobilization method	Aptamer label and amplification strategy	Detection strategy	Analytical parameters* (Linear range (LR), detection limit (LOD), sensitivity, specificity, recovery rate) in pristine electrolyte and in real sample.	Comparison with standard techniques
BoIFN-γ [60] (SWV; turn-off)	GDE/3′ thiol; SAM	-5′ MB label	-Switching of aptamer hairpin	In HEPES pH 7.4: 2.2 ng mL^{-1} (0.1 nM) LOD; 1–230 ng mL^{-1} LR In whole blood and in RPMI/10% serum: 14 ng mL^{-1} and 15.7 ng mL^{-1} LOD, respectively (matrix effect observed). LOD equation (not specified)	-NA
IFN-γ [63] (SWV; turn-off)	Au microarray/3′ thiol; SAM	-5′ MB label	-Switching of aptamer hairpin	In PBS pH 7.4: 1.3 ng mL^{-1} LOD; 1–500 ng mL^{-1} LR In RPMI/10% serum (parameters NR) LOD equation: 3 × SD	-NA
IFN-γ [62] (SWV; turn-off)	Au coated SiNWs/3′ thiol; SAM	-5′ MB -Gold/SiNWs	-Switching of aptamer hairpin	In HEPES pH 7.4: 0.14 ng mL^{-1} LOD; 0.2–80 ng mL^{-1} LR. LOD equation: S/N of 3 In PBMC/RPMI/10% serum: IFN-γ detected in 150 T cells mL^{-1}. Improved performance than ELISA due to co-location of cells close to sensor surface	-ELISA 3–90 pg mL^{-1} LR (5000-30000 T-cells)
HspX [87] (DPV; turn-off)	AuNPs-SPCE/3′ thiol; SAM	-5′ MB -AuNPs sensing platform	-Switching of aptamer hairpin	In Tris buffer pH 7.5: 10 pg mL^{-1} LOD; 0.01–500 ng mL^{-1} LR. LOD equation (not specified) in 10% CSF samples/Tris buffer pH 7.5: Sensitivity (~95%), specificity (~97.5%), LOD of 10 pg mL^{-1}	-TB confirmed via culture, smear, commercial NAAT positive and acid-fast bacillus (AFB)
MPT64 [79] (DPV; turn-on)	PEI-Fe-MOF/Au@Pt-GCE/5′ thiol; SAM	-Au-C_{60}NPs-N-CNTs/GO label -PEI-Fe-MOF -TOAB	-Sandwich assay	In PBS pH 7.0: 0.33 fg mL^{-1} LOD; 1 fg mL^{-1} –1 ng mL^{-1} LR. LOD equation (not specified) In 2% clinical healthy human serum: 94.8%–102.0% recovery, In TB infected serum (Recovery NR)	-Method of TB confirmation for infected samples (not specified), 100% sensitivity
MPT64 [82] (DPV; turn-on)	GDE/5′ thiol; SAM	-GNPs-C_{60}-PAn label	-Sandwich assay	In PBS pH 7.0: 20 fg mL^{-1} LOD; 0.02–1000 pg mL^{-1} LR/ LOD equation: 3 × SD_{blank}/$slope_{calibration\ curve}$ In healthy human serum: 97.28%–107.3% recovery	-Method of TB confirmation in infected samples (not specified), 100% sensitivity
MPT64 [80] (DPV; turn-on)	GDE/5′ thiol; SAM	-Au@PB-HRP label	-Sandwich assay	In PBS pH 7.0 + HQ + H_2O_2: 21 fg mL^{-1} LOD; 1–10,000 pg mL^{-1} LR. LOD equation: 3 × SD In human serum: 97.4%−110% recovery	-NA
MPT64 [81] (DPV; turn-on)	GDE/5′ thiol; SAM	-AuNPs/MOF label -HRP	-Sandwich assay	In PBS pH 7.0 + HQ + H_2O_2: 10 fg mL^{-1} LOD; 0.02–1000 pg mL^{-1} LR. LOD equation: 3 × SD In healthy human serum: 95.9%−111.6% recovery	-NA

All the aptasensors listed above are reagentless. NR (Not reported, experiments were performed but analytical parameter not stated). NA (Not applicable, experiments not performed). SD (Standard deviation). For ease of comparison, where concentrations were reported in the original source document in molarity (M) rather than mass concentrations (g mL^{-1}), conversions were made using the biomarker molecular weights. IFN-γ = 17 kDa [117,118]; MPT64 = 46 kDa [119]; Ag85A = 34.1 kDa . RSD = relative standard deviation; SD = standard deviation; RD = relative difference; Sm = standard deviation of blank signal; k = multiple constant for random error and equal to 3; m = slope of linear fit; Cm = detection limit; MDL is method detection limit; tv,α is the student's t value at v degrees of freedom and α confidence level of 1%; S/N = signal-to-noise ratio. This applies to all Tables.

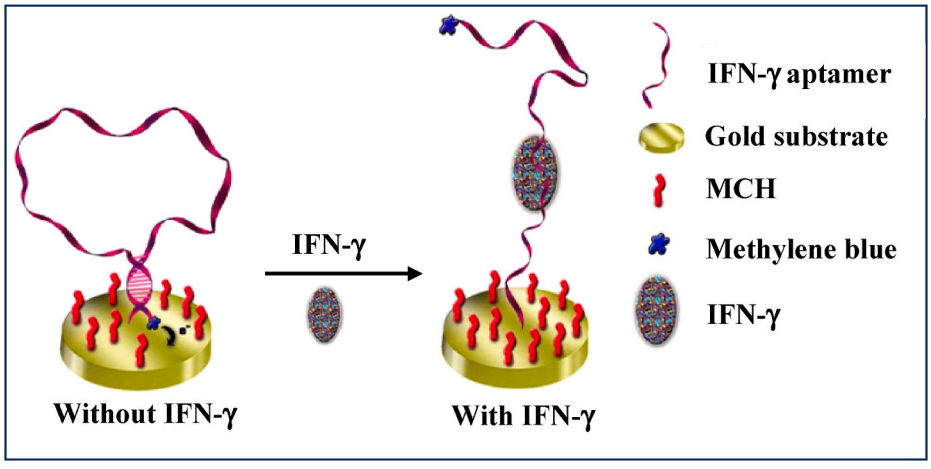

Fig. 4. Schematic diagram of MB tagged IFN-γ aptamer, before and after target [63]. Figure adapted with Copyright permission (2014) Elsevier.

0.9 fg mL^{-1} LOD with 5′ biotinylated aptamer, using streptavidin graphene-iron-oxide chitosan hybrid (CHIT-IOGR) nanocomposite-modified FTO electrode [86].

Electrochemical surface enhanced Raman spectroscopy (EC-SERS) is an advanced analytical technique which combines electrochemical and surface enhanced Raman spectroscopic techniques to measure changes in Raman scattering intensity of molecules immobilized on solid surfaces [122]. An aptasensor for IS6110 of MTB DNA with LOD of 280 μg mL^{-1} in synthetic urine samples was reported using adenine-containing IS6110 target strand and adenine-free aptamer probe strand [94]. The aptamer was immobilized on AgNPs-modified SPCE by Ag–S SAM. DNA hybridization, and MTB DNA quantification were determined by the appearance of adenine marker bands at 730 cm^{-1} and 1330 cm^{-1}.

Field-effect transistors (FET) aptasensors are based on measurement of changes of source-drain current against chosen gate voltage as a result of binding of molecules, using agilent semiconductor parameter analyzer. A graphene monolayer-based label-free FET-like IFN-γ aptasensor was fabricated by Farid et al. (2015). Detection, to LOD of 83 pM,

Table 4
Label-free electrochemical and piezoelectrical-based aptasensors for TB biomarkers.

Target	Electrode/ immobilization method	Probe label and amplification strategy	Detection strategy	Analytical parameters* (linear range (LR), detection limit (LOD), sensitivity, specificity, recovery) in pristine electrolyte and in real sample	Comparison with standard techniques
IFN-γ [78] (SWV; turn-on)	Au microgap/5′-thiol, SAM	-Intercalated Ag redox probe	-Dissociation of aptamer structure	In HEPES buffer pH 7.03: 0.67 pg mL^{-1} LOD; 1 pg mL^{-1}–10 ng mL^{-1} LR. In HEPES buffer/10% human serum samples: 0.42 pg mL^{-1} LOD; 1 pg mL^{-1}–10 ng mL^{-1} LR. LOD equation (not specified)	-NA
IFN-γ [58] (DPV; turn-off)	SPGEs/3′-STP; hybridization	-Intercalated MB redox probe	-Dissociation of THMS system	In PBS buffer: 3 pg mL^{-1} LOD; 10–1500 pg mL^{-1} LR In PBS/10% human serum: 91.3%–102.8% recovery LOD equation: > blank + 3RSD	-NA
IFN-γ [66]; (turn-off) Lys (turn-on); SWV	GDE/5′ thiol SP; hybridization	Fc–IFN–γ and MB-Lys signal probes	-Dissociation of aptamer/SP duplex	In Tris buffer pH 7.4: 19.38 pg mL^{-1} (1.14 pM) IFN-γ LOD; 0.17–170 ng mL^{-1} (0.01–10 nM) IFN-γ LR In Tris-HCl 7.4/300-fold diluted human serum from healthy humans: 92.80%−104.0% IFN-γ recovery LOD equation: S/N of 3	-NA
IFN-γ [68] (EIS; turn-on)	AuIDE/5′ thiol; SAM	–	-Change in impedance	In PBS pH 7.0 + $[Fe(CN)]^{3-/4}$: 0.91 ng mL^{-1} (20.22 pM) LOD; 1–10 ng mL^{-1} (22.22 pM–0.22 nM) In FBS: 0.52 ng mL^{-1} (11.56 pM) LOD; 1–5 ng mL^{-1} (22.22 pM–0.11 nM). LOD equation: $MDL = t_{\nu,\alpha.} \times SD$	-NA
MPT64 [83] (EIS; turn-on)	GDE/5′ thiol; SAM	–	-Change in impedance	In SELEX buffer/1% human serum: 3.7 ng mL^{-1} (81 pM) LOD; 2.26–ng mL^{-1}–2300 ng mL^{-1} (49 pM–50 nM) LR LOD equation: mean blank + 1.645(SD_{blank}) + 1.645($SD_{low\ concentration\ sample}$)	-NA
MPT64 [84] (EIS; turn-on)	Au-IDE/5′ thiol; SAM	–	-Change in impedance	LOD: 188.6 fg mL^{-1} (4.1 fM); LR: 4.6 fg mL^{-1}–230 ng mL^{-1} (0.1 fM–5 nM) In sputum/$[Fe(CN)_6]^{3-/4-}$: 76.47% sensitivity; 100% specificity. In serum/$[Fe(CN)_6]^{3-/4-}$: 82.24% sensitivity 100% specificity (relative to AFB) LOD equation: mean blank + 1.645(SD_{blank}) + 1.645($SD_{low\ concentration\ sample}$)	- Acid fast bacilli (AFB) staining: Reduced sensitivity due to matrix effect
IFN-γ [55] (DSPV; turn-on)	-GCE	-AuNPs -DNAzyme -SA-$Cu_3(PO_4)_2$–HNF-G	-Structure switching of DDAH	In 0.1 M HCl: 19 fg mL^{-1} LOD; 0.1 pg mL^{-1}–500 ng mL^{-1} LR In 10% human serum: 95.26%–109.91% recovery LOD equation (not specified)	-NA
IFN-γ [69] (LSV; turn-on)	GDE/5′ thiol; SAM	-hairpin self-assembly -(+)AgNPs reporter	switching of aptamer hairpin	In KCl: 9.69 pg mL^{-1} (0.57 pM) LOD; 17–8500 pg mL^{-1} (1–500 pM) LR In human serum: 94.75–102.63% recovery LOD equation: mean blank response + 3SD	-NA
IFN-γ [70] (DPV; turn-on)	Nf/(+)AuNPs-GDE/3′ CP thiol; SAM	-HCR -Nf/(+)AuNPs platform - Ir(III) complex	-Switching of CP stem-loop structure	In PBS pH 7.0: 277.1 fg mL^{-1} (16.3 fM) LOD; 850 fg mL^{-1}–51 pg mL^{-1} (50 fM–3 pM) LR In PBS/1% human serum in 96.6%–108% recovery LOD equation: 3 × $SD_{blank}/slope_{calibration\ curve}$	-NA
IFN-γ [71] (SWV; turn-on)	GCE-AuNPs-PAMAM-MoS_2-GCE/3′ thiol; SAM	-AuNPs/PAMAM/MoS_2 -MB redox probe	-Switching of aptamer hairpin	In PBS pH 7.4: 2 fg mL^{-1} LOD; 0.01–1000 pg mL^{-1} LR In PBS pH 7.4/10% real human serum and in PBS pH 7.4/10% urine sample: 95.2%–105.0% and 95.2–100.4% recoveries, respectively. LOD equation: S/N of 3	ELISA (comparable result)
ESAT6 [91] (CV; turn-off)	Pt@AuNPs-GCE/5′ thiol; SAM	-Pt@AuNPs platform -PDDA-MOF-rGO -Toluidine blue reporter	-Change in impedance	In PBS pH 7.0 + KCl + $MgCl_2$: 0.33 fg mL^{-1} LOD; 10 pg mL^{-1}–200 ng mL^{-1} LR In clinical healthy human serum: 99–102% recovery LOD equation: 3 × $SD_{blank}/slope_{calibration\ curve}$	-NA
ESAT6 [92] (CV; turn-off)	NG@Zr-MOF-on-Ce-MOF@Tb-GCE/5′-PO_4^{3-}	-NG@Zr-MOF-on-Ce-MOF platform -Toluidine blue reporter	-Change in impedance	In PB pH 7.0: 12 fg mL^{-1} LOD; 100 fg mL^{-1}–10 ng mL^{-1} LR In 50% diluted healthy human serum: 90–94.3% recovery LOD equation: 3 × $SD_{blank}/slope_{calibration\ curve}$	-Method of TB confirmation in infected samples (not specified). 100% sensitivity
CFP10-ESAT6 [89] (DPV; turn on)	GP/PANI-SPGE/5′-NH_2; Glutaraldehyde crosslinker	-GP/PANI platform -Fe_3O_4/Au MNPs reporter	-Aptamer-Antibody sandwich assay	In PBS pH 7.4 + H_2SO_4: 1.5 ng mL^{-1} LOD; 5–500 ng mL^{-1} LR In healthy and infected sputum samples: 100% sensitivity and specificity relative to	- Sputum smear microscopy and culture method.

(*continued on next page*)

Table 4 (*continued*)

Target	Electrode/ immobilization method	Probe label and amplification strategy	Detection strategy	Analytical parameters* (linear range (LR), detection limit (LOD), sensitivity, specificity, recovery) in pristine electrolyte and in real sample	Comparison with standard techniques
				culture and smear microscopy methods. LOD equation: 3 × $SD_{blank}/slope_{calibration\ curve}$	
MPT64 [85] (DPV; turn-on)	Streptavidin-PEDOT-CNT-FTO/5′ biotin-aptamer	PEDOT-CNTs sensing platform	-Change in impedance	In PBS pH 7.0 + $[Fe(CN)_6]^{3-/4-}$: 0.5 ± 0.2 fg mL^{-1} LOD; 1 pg mL^{-1}–10 ng mL^{-1} LR. Sensitivity of 176 μA fg mL^{-1} cm^{-2} In human serum: 88%–95% recovery (matrix effect) LOD equation: 3 × $SD_{blank}/slope_{calibration\ curve}$	-LOD of 0.1 fg mL^{-1} (culture method); 10 ng mL^{-1} (ELISA); 12.35 ng mL^{-1} (commercial immunochro-matographic test)
MPT64 [86] (DPV; turn-on)	Streptavidin-CHITIOGR- FTO/5′ biotin Aptamer	CHIT-IOGR nanocomposite film sensing platform	-Change in impedance	In PBS pH 7.0 + $[Fe(CN)_6]^{3-/4-}$: 0.9 fg mL^{-1} LOD; 1 fg mL^{-1} –10 ng mL^{-1} LR. Sensitivity of 100 μA fg mL^{-1} cm^{-2} In human serum: 83–95% recovery (matrix effect). LOD equation: 3 × $SD_{blank}/slope_{calibration\ curve}$	-NA
IS6110 [94] (EC-SERS; turn-on)	-AgNPs sensing platform	-AgNPs	-Change in Raman scattering intensity	In 0.1 M NaF: 280 μg mL^{-1} LOD; LR (NR) In synthetic urine: (Parameters NR) LOD equation (not specified)	-NA
IFN- γ [72] (FET; turn-on)	Graphene platform; π-π interaction	-Graphene	-Change in electrolyte charge distribution	In PBS: 1.41 ng mL^{-1} (83 pM) LOD; 34 ng mL^{-1}–170 μg mL^{-1} (2 nM–10 μM) LR LOD determined from instrumental (HP 4155C parameter analyzer) resolution limit	-NA
IFN-γ [120] (FET/ISVR; turn-on)	Graphene platform; π-π interaction	-Graphene	-Change in electrolyte charge distribution	LR: < 170 ng mL^{-1} (<10 μM) LOD determined from instrumental (HP 4155C parameter analyzer) resolution limit.	-NA
IFN-γ [73] (DPV; turn-on)	Graphene-AuNPs-GCE/5′ thiol; SAM	-Grapene-AuNPs -RecJf EATR -SA-ALP	Dissociation of aptamer/CP duplex	In DEA buffer pH 9.6: 34 pg mL^{-1} (2 pM) LOD; 85 pg mL^{-1} –85 ng mL^{-1} (5 pM–5 nM) LR In DEA buffer pH 9.6/human serum: 91.3%–107.7% recovery compared to ELISA. LOD equation: S/N of 3	ELISA (recovery 91.3%–107.7% relative to ELISA)
IFN-γ [57] (DPV; turn-on)	AuNPs-Graphene-GCE/5′ CP thiol; Hybridization	-AuNPs-Graphene - Au@Fe_3O_4-SP -RecJf and TdT EATRS	Dissociation of aptamer/SP duplex	In PBS pH 7.0: 3 pg mL^{-1} LOD; 0.01–50 ng mL^{-1} LR In PBS pH 7.0/clinical human serum samples: 0.38–5.03 ng mL^{-1} LR LOD equation: 3 × $SD_{blank}/slope_{calibration\ curve}$	ELISA (Recovery of 0.41–5.37 ng mL^{-1},<10.1% RD compared to aptasensor)
IFN-γ [74] (DPV; turn-on)	GDE/Aptamer -Graphene; π-π interaction	-DNase 1 -Graphene reporter	Dissociation of aptamer- graphene assemble	In PBS pH 7.0 + FcCOOH + $NaClO_4$: 1.1 pg mL^{-1} (0.065 pM) LOD; 7–11.9 pg mL^{-1} (0.1–0.7 pM) LR In RPMI/10% fetal bovine serum (Parameters: NR) LOD equation: 3 × SD	-NA
IFN-γ [75] (EIS; turn-on)	GDE/3′ thiol; SAM	-EATR (Exo I and III)	-Switching of aptamer hairpin	In $[Fe(CN)]^{3-/4}$ + KCl: 11.9 pg mL^{-1} (0.7 pM) LOD; 17 pg mL^{-1}–850 ng mL^{-1} (1 pM–50 nM) LR In human serum: 91.83%–101.90% recovery LOD equation: S/N of 3	ELISA (Recovery 94.54%–98.35%)
IFN-γ [76] (DPV; turn-on)	-GDE/5′ thiol; SAM	-HCR -SA–ALP redox reporter	-Switching of DNA hairpins for HCR	In Tris buffer pH 9.6: 5.1 ng mL^{-1} (0.3 nM) LOD; 8.5–5100 ng mL^{-1} (0.5–300 nM) LR In RPMI/10% serum (Parameters NR) LOD equation: 3 × SD	-NA
IFN-γ [77] (CV; turn-on)	GDE/3′ thiol; SAM	-DNAzyme formation	-Switching of aptamer hairpin	In HEPES pH 7.4: 1.7 ng mL^{-1} (0.1 nM) LOD: LR (NR) LOD equation: (NR)	-NA
CFP10 [121] (CA; turn on)	diazonium salt –COOH–SPCE/5′-thiol; EDC/NHS	-HRP reporter	Aptamer-antibody sandwich assay	PBS pH 7.4 + H_2O_2 + HQ: 1.22 ng mL^{-1} LOD; 5–500 ng mL^{-1} LR In human serum: 1.05 ng mL^{-1} LOD; 2.5–250 ng mL^{-1} LR LOD equation: 3 × $SD_{blank}/slope_{calibration\ curve}$	-NA
CFP10 [90] (DPV; turn-on)	GDE/5′(DBCO)-DNA thiol; Hybridization	-AuNPs-DNA -Hybridization -DNAzyme and HRP	-Dissociation of aptamer/CP dsDNA	In PBS pH 7.4 + HQ + H_2O_2: 10 pg mL^{-1} LOD; 0.01–100 ng mL^{-1} LR In clinical healthy and TB infected sputum samples (Parameter: %recovery NR) LOD equation: S/N of 3	-ELISA (100% sensitivity compared with ELISA)
H37Rv [93] (MSPQC; turn-on)	Au-IDE/5′ thiol; SAM	SWCNTs	Dissociation of aptamer/SWCNTs composite	In detection medium: 100 cfu mL^{-1} LOD; LR (NR) In detection medium/20% clinical sputum samples: 86% sensitivity; 90% specificity relative to culture method, and 100% sensitivity; 91% specificity relative to BACTEC MGIT 960 automated system LOD equation: 3 × $SD_{blank}/slope_{calibration\ curve}$	-Culture method -BACTEC MGIT 960 automated system - + TB confirmed by acid-fast smear analysis.
CFP10-ESAT6 [88] (MSPQC; turn-on)	Au-IDE/3′ thiol CP-AuNPs; Hybridization	AuNPs-capture probe	Dissociation of aptamer/CP dsDNA Duplex	In $[Fe(CN)_6]^{3-/4-}$ LOD and LR (NR) In M7H9 culture medium/clinical pathogenic MTB sample: 10^3 cfu mL^{-1} LOD LOD equation (not specified)	-NA

All the aptasensors listed above are reagentless. RSD = relative standard deviation; SD = standard deviation; RD = relative difference; Sm = standard deviation of blank signal; k = multiple constant for random error and equal to 3; m = slope of linear fit; Cm = detection limit; MDL is method detection limit; tv,α is the student's t value at v degrees of freedom and α confidence level of 1%; S/N = signal-to-noise ratio.

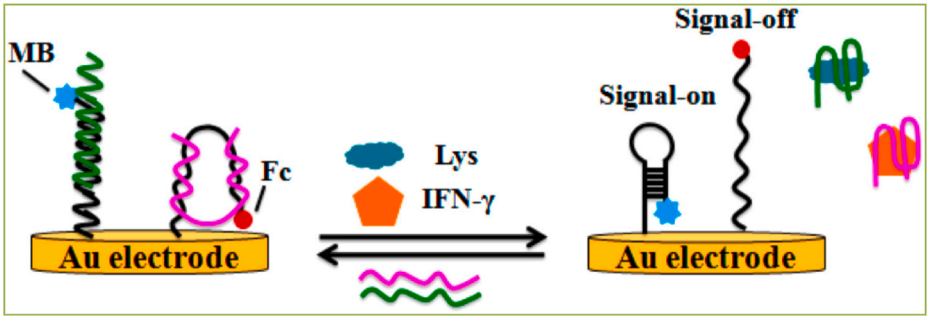

Fig. 5. A multiplex aptasensor schematic for IFN-γ and TNF-α. Reproduced from Xia et al., [66] with Copyright permission (2015) Elsevier.

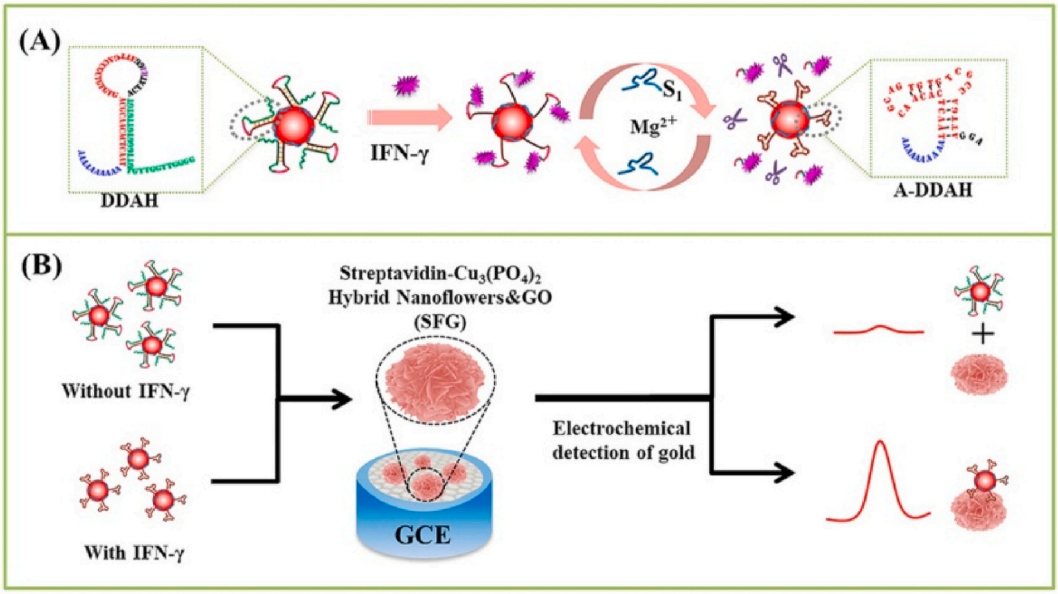

Fig. 6. Schematic representation of SFG-based aptasensor for IFN-γ.showing (A) the target-triggered allosteric switching and (B) its detection principle [55]. Copyright permission (2019) Elsevier.

is based on change in electrolyte charge distribution on target binding, resulting in increased electron transfer efficiency [72]. Akbari et al. (2016) used Incremental Support Vector Regression (ISVR) algorithm as a method of improvement of prediction accuracy, to support the current–voltage characteristic of their graphene-based FET aptasensor [120].

2.2.2. *Enzyme-assisted label-free electrochemical TB aptasensors*

An improvement of the PCR-based nucleic acid amplification technique offer enzyme-assisted target recycling strategy (EATRS) for amplifying response. This uses an enzyme, usually a nuclease, for recognition of target-probe complex and probe digestion for target release/recycle. The released target then binds to another probe, thereby increasing the target response. For instance, RecJf exonuclease, an enzyme specific for the catalytic removal of deoxy-nucleotide monophosphates from single stranded-DNA in the 5'→3′ direction has been reported for a label-free "signal-on" IFN-γ aptasensor. This aptasensor with LOD of 2 pM uses graphene/AuNPs-modified GCE as sensing platform for immobilization of hybridized aptamer/capture probe duplex, and RecJf exonuclease for aptamer digestion [73]. Target binding causes dissociation of the aptamer/capture probe duplex, initiating selective digestion of aptamer by RecJf exonuclease, release/recycle of IFN-γ, and subsequent hybridization of single strand DNA with linker probes and biotin-labeled reporter probe. A similar label-free IFN-γ aptasensor was reported using RecJf exonuclease and terminal deoxynucleotidyl transferase (TdT) enzymes. This aptasensor which also incorporated AuNPs-graphene nanocomposite (Au-Gra)-modified GCE sensing platform, $Au@Fe_3O_4$ signal probe (SP) label, and $[Ru(NH_3)_6]^{3+}$ redox reporter, achieved LOD of 0.003 ng mL^{-1} [57]. Aptamer/SP dsDNA immobilized on the Au-Gra-modified GCE was dissociation on target binding. Selective digestion of aptamer and release of IFN-γ was achieved using RecJf exonuclease, while terminal deoxynucleotidyl transferase (TdT) ensured catalytic addition of nucleotide to the 3′ terminus of the SP suitable for increased loading of the $[Ru(NH_3)_6]^{3+}$. Deoxyribonuclease I (DNase 1), an endonuclease capable of cleaving single stranded (ssDNA), double stranded DNA (dsDNA) and chromatin, predominantly at the 5′ phosphodiester linkages has been reported for a "signal-on" label-free IFN-γ aptasensor with LOD of 0.065 pM as shown in Fig. 7 [74]. In this work, label-free IFN-γ aptamer was adsorbed on graphene reporter molecules by π-π stacking interaction. Target binding

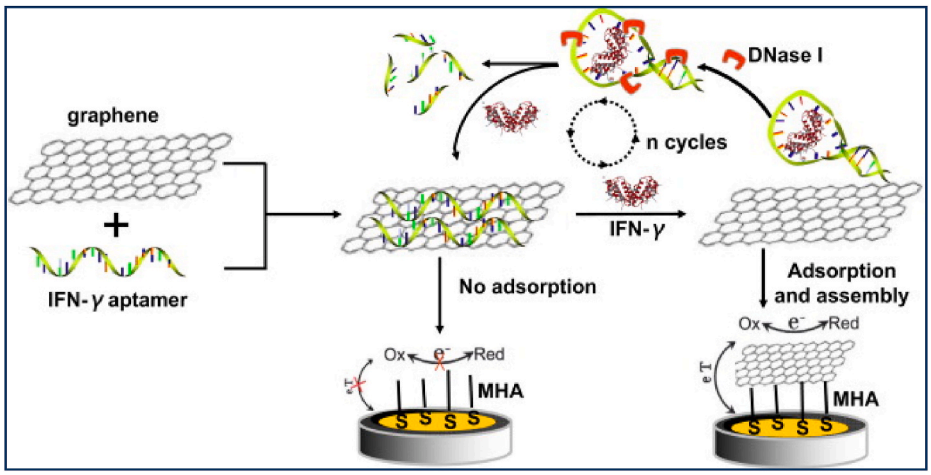

Fig. 7. Electrochemical aptasensor for the IFN-γ detection based on graphene controlled assembly and DNase 1 EATRS reproduced from Yan et al. [74], Copyright permission (2013) Elsevier.

released the graphene onto a 16-mercaptohexadecanoic acid-modified GDE leading to increased signal. DNase 1 enzymatic cleavage of the aptamer initiated cycles of target release and recycling. In another format, inhibition of exonuclease digestion of aptamer hairpin structure on target binding was reported for an IFN-γ "turn-on" impedimetric aptasensor with LOD of 0.7 pM [75]. In this case, selective digestion of the single-stranded and double-stranded regions of the IFN-γ aptamer hairpin structure were achieved with exonuclease I (Exo I) and exonuclease III (Exo III), respectively, only in the absence of IFN-γ.

As label molecules, enzymes such as DNAzyme, alkaline phosphatase (ALP) and horseradish peroxidase (HRP) are used as redox probes for electrochemical-based aptasensors. For instance, Zhao et al. (2012) reported a HCR-based IFN-γ aptasensor, which uses a streptavidin-labeled ALP (SA-ALP) for catalytic oxidation of electro-inactive 1-naphthyl phosphate to electroactive 1-naphthol [76]. DNAzymes are catalytic ssDNA which can perform specific chemical reactions. Peroxidase mimicking DNAzyme, formed by the association of the G-quad sequence of the DNAzyme with hemin, catalyzes the electrochemical reduction of hydrogen peroxide (H_2O_2). In one application, Zhang et al. (2012) fabricated a "turn-on" IFN-γ aptasensor using label-free IFN-γ aptamer containing specific DNAzyme sequence. In this case, switching of aptamer hairpin structure on target binding led to formation of G-quad peroxidase mimicking DNAzyme with the aid of hemin, which catalyzes the electro-reduction of H_2O_2 to give 0.1 nM LOD [77]. Recently, a HRP-tagged antibody reporter probe for the reduction of hydroquinone (HQ), together with an aptamer signal probe, has been reported for a turn-on amperometric sandwich assay CFP10 biosensor with LOD of 1.22 ng mL^{-1} [121]. Li et al. (2019) reported a "turn-on" aptasensor for CFP10 antigen with LOD of 10 pg mL^{-1} based on DNA recycling and click reaction triggered by an azido-terminated DNA (N_3-DNA) complementary sequence. Binding of target induced dissociation of the dsDNA and recycling of CFP10 target. This is followed by hybridization of the aptamer with AuNPs-DNA and formation of G-quad DNAzyme in the presence of hemin [90].

3. Piezoelectric aptasensors for TB biomarker

Piezoelectric quartz crystal (PZQC) aptasensors are electromechanical aptasensors that measure changes in the oscillating frequency of a piezoelectric material resulting from biochemical response due to aptamer/target recognition. The target-specific aptamers are usually immobilized on a quartz crystal microbalance (QCM) coated on both sides with a magnetic material and coupled to an oscillating circuit. Oscillation is induced in the center of the QCM by applying alternating electrical field from the oscillating circuit [123], with frequency dependent on the magnitude of the applied electricity. Binding of target to aptamer causes increase in the mass of the QCM, and/or changes in solution resistance and capacitance with corresponding changes in the oscillation frequency of the QCM, which is monitored by a frequency counter. Multichannel-series piezoelectric quartz crystal (MSPQC) is a type of series PZQC which allows for simultaneous analysis of multiple samples. MSPQC-based aptasensors have been reported for TB biomarkers with detection based on the displacement of signal indicators, usually conductive materials such as single-walled carbon nanotubes (SWCNTs) [93] and AuNPs-labeled complementary oligonucleotide probe (DNA-AuNPs) [88], by non-conductive target molecule on target binding. This leads to change in electrical properties, and is recorded as changes in frequency shift. Using DNA-AuNPs for fused CFP10-ESAT6 aptasensor with LOD of 10^3 cfu mL^{-1}, the aptamer was first hybridized with the DNA-AuNPs prior to immobilization on AuIDE [88]. While on the other hand, using SWCNTs for a H37Rv aptasensor with LOD of 100 cfu mL^{-1} [93], a label-free thiolated aptamer immobilized on AuIDE was bonded to the SWCNTs by π-π interaction.

4. Optical TB aptasensors

Optical aptasensors are aptasensors that employ optical transducers to measure changes in properties of light resulting from aptamer-target biorecognition. Optical-based detection techniques depend on the particular light property being measured, such as changes in light absorption (colorimetric technique), emission (luminescence, chemiluminescence and fluorescence techniques), refractive index (surface plasmon resonance technique) and polarization (polarized light microscopy). Colorimetric (Col.) aptasensors are based on changes in the wavelength and/or intensity of light absorption which occur in the ultraviolet or visible regions of the electromagnetic spectrum. Though generally insensitive, their advantage lie in their inexpensive nature as target can be directly detected with the naked eyes without the need for expensive analytical equipment [124]. Chemiluminescence (CL) aptasensors offer an optical detection based on changes in light emission resulting from changes in biochemical reactions due to aptamer-target interaction. Fluorescence (FL)-based aptasensors are rapid and robust, with high selectivity and sensitivity. However, most FL aptasensors require fluorophore-labels which might cause interference due to their susceptibility to self-quenching, photo-bleaching, and pH dependence. Surface plasmon resonance (SPR) technique has become increasingly important in biomolecular imaging and study of biomolecular interactions due to its real-time, non-invasive and label-free characteristics. This technique generates surface plasmons by absorption of light photons formed when incident light hits a metal-dielectric interface at

total internal reflection. SPR occurs when the momentum of the incident light is equal to the momentum of the surface plasmon at appropriate energy and angle of incidence. Hence, SPR-based measurement can be made as changes in refractive index [125], resonant angle and wavelength [36], intensity of reflected light and phase shift resulting from formation of aptamer-target complex.

4.1. Label-based optical TB aptasensors

Optical-based techniques have been employed for label-based TB aptasensors (Table 5). Label-based FL aptasensors are designed to monitor changes in FL emission as a result of aggregation of label molecules on target binding. Aggregation induced emission (AIE) mechanism is one format of FL detection based on the principle of increase in FL emission as a result of restriction of intramolecular rotation of AIEgens molecules on aggregation. Its advantages include relative immunity to fluorescent quenching and their characteristic high brightness. Ma's group based their IFN-γ aptasensor on this mechanism using an IFN-γ aptamer linked to an azide group-modified AIEgen (tetraphenyl ethylene molecule, TPE). This TPE-aptasensor achieved LOD of 2 pg mL^{-1} [95]. In another format, the fluorescent enhancement of fluorescein, BODIPY, TAMRA and Alexa Fluor 488 aptamer fluorescent labels were monitored for IFN-γ and Adenine biomarkers [96]. Though the aptamers were quencher-free, FL quenching was estimated to occur by photoinduced electron-transfer (PET) process of the spatial neighboring G bases of the aptamer in the presence of target, but was recovered on target binding due to changes in the PET efficiency. In this study, the highest FL enhancement was recorded with BODIPY-labeled aptamer.

4.1.1. Nanomaterials as labels and sensing platforms for increased sensitivities of TB optical aptasensors

Nanomaterials have found wide range of application in optical-based TB aptasensors due to their favorable properties. As label molecules, nanomaterials offer many advantages over organic fluorophores. These advantages include photo- and chemical stability, inertness, and reduced to none cytotoxicity. The use of graphene-based nanomaterials such as graphene quantum dots (GQDs) and graphene oxide (GO) nanomaterials in FL aptasensors lie in their quenching capabilities in addition to their nanomaterial characteristics. For instance, using FL GQDs-linked aptamer (Ap-GQDs) and GQDs-linked epitope (Ep-GQDs), Liu's group achieved aggregation and FL quenching due to hybridization of Ap-GQDs and EP-GQDs in the absence of IFN-γ, and its recovery in the presence of IFN-γ due to disaggregation of the conjugate [97]. Exploring the FL quenching and DNA adsorption capability of GO, as well as its ability to reduce background noise, a recent fluorescence resonance energy transfer (FRET)-based aptasensor has been reported for TB7.7 aptasensor with LOD of 0.8779 nM in buffer, and 0.7089 nM in clinical samples [113]. FRET-based FL quenching was achieved in the absence of target due to preservation of the aptamer hairpin and the resulting close proximity of the FAM to BHQ1 quencher. Switching of the aptamer hairpin structure in the presence of target led to FL regeneration. In another report, using GO sensing platform, FL quenching of ATTO647N-labeled Ag85A aptamer adsorbed on GO by hydrophobic π-π interaction was observed in the absence of target, and restored in the presence of Ag85A giving LOD of 1.5 nM [112]. Based on the same format, a lower LOD of 1.5 fM was obtained by incorporating polymerase-based EATR [98]. In this case, in the presence of target, primer and polymerase, switching of the FAM-labeled aptamer hairpin structure occur, triggering strand-displacement polymerization amplification strategy and FL recovery. Also, a "turn-on" FL aptasensor based on 2D ReS_2 and TiS_2 chalcogenide nanosheets sensing platform for immobilization of FAM-labeled IFN-γ aptamer was recently reported with LOD of 57.6 and 82.7 pM for ReS_2 and TiS_2, respectively [99]. Detection was attributed to changes in FRET between the FAM-labeled aptamer and the chalcogenide nanosheets. This results to FL quenching in the absence of target, and its recovery in the presence of IFN-γ.

4.2. Label-free TB optical aptasensors

The most common assay format reported for label-free TB optical aptasensors is structure-switching of aptamer G-quadruplex (G-quad) or hairpin structures on target binding (Table 6). In the presence of target, formation of aptamer-target duplex disrupts the G-quad structure, leading to measurable changes in the microenvironment of the system.

Table 5
Label-Based Optical Aptasensors for TB biomarkers.

Target	Aptamer label and signal amplification	Detection strategy	Analytical parameters* (linear range (LR), detection limit (LOD), sensitivity, specificity, recovery) in pristine medium and in real sample	Comparison with standard techniques
IFN-γ [95] (FL; turn-on)	-TPE label	Aggregation/ disaggregation	In PBS pH 7.4: 2 pg mL^{-1} LOD; 0–100 pg mL^{-1} LR. Imaging with BV2 and PBMC. LOD equation: S/N of 3	ELISA (confirms real-time bioimaging with BV2 cells)
IFN-γ [96] (FL; turn-on)	-BODIPY-FL-NHS; TAMRA; Alexa Fluor 488 label	change in PET process	In electrolyte: LOD and LR (NR). Imaging with CCRF-CEM cells. LOD equation (not specified)	-NA
IFN-γ [97] (FL; turn-on)	GQDs label	Aggregation/ disaggregation	In PBS pH 7.4: 2 pg mL^{-1} LOD; 5–100 pg mL^{-1} LR. Imaging BV2 and PBMC. LOD equation: S/N of 3	ELISA: confirms IFN-γ uptake by BV2 cells.
TB7.7 [113] (FL; turn on)	FAM label GO quencher	Change in FRET	In buffer: 6.76 ng mL^{-1} (0.8779 nM) LOD; 7.7–2310 ng mL^{-1} (1 nM–300 nM) LR. In 10% human serum: 5.46 ng mL^{-1} (0.7089 nM) LOD; 7.7–2310 ng mL^{-1} (1 nM–300 nM) LR. LOD equation (not specified) In clinical active TB serum samples: 41.67% sensitivity; 92.86% specificity relative to AFB (matrix effect);	TB confirmed with culture method and acid-fast bacillus (AFB) staining.
Ag85A [112] (FL; turn-on)	- ATTO647 N -GO quencher	Change in aptamer hairpin	In PBS: 51.2 ng mL^{-1} (1.5 nM) LOD; 170.5–6820 ng mL^{-1} (5–200 nM) LR. LOD equation: $3 \times SD_{blank}/slope_{calibration\ curve}$ In 2% healthy human serum: 91.8–97% recovery; 2.1 nM LOD.	-NA
IFN-γ [98] (FL; turn-on)	-FAM -GO quencher -Polymerase	Change in aptamer hairpin	In PBS: 25.5 fg mL^{-1} (1.5 fM) LOD; 59.5 fg mL^{-1}–17 pg mL^{-1} (3.5 fM–1.0 pM) LR. LOD equation (not specified) In human plasma samples: 87.6%–92.8% recovery	-NA
IFN-γ [99] (FL; turn-on)	-FAM -2D ReS_2 and TiS_2 nanosheets platform	Change in FRET	In PBS pH 7.4: 979.2 pg mL^{-1} (57.6 pM) LOD and 0–400 pg mL^{-1} LR for ReS_2 NS; 1.4 ng mL^{-1} (82.7 pM) LOD; 0–300 pg mL^{-1} LR for TiS_2. LOD equation: $3 \times SD_{blank}/slope_{calibration\ curve}$ Imaging in live HEK cells	-NA

All the aptasensors listed above are reagentless.

Table 6
Label-Free Optical Aptasensors for TB biomarkers.

Target	Signal amplification strategy	Detection strategy	Analytical parameters* (linear range (LR), detection limit (LOD), sensitivity, specificity, recovery) in pristine medium and in real sample	Comparison with standard techniques
IFN-γ [102] (FL; turn-on)	thiazole orange (TO) redox reporter	-Change in G-quadruplex aptamer structure	In Tris-HCl 7.4: 34 ng mL^{-1} (2.0 nM) LOD; 51–2040 ng mL^{-1} (3.0–120 nM) LR. In healthy human serum: 98–107% recovery LOD equation: 3 × $SD_{blank}/slope_{calibration\ curve}$	-NA
IFN-γ [103] (FL; turn-off)	thioflavin T redox reporter	-Change in G-quadruplex aptamer structure	In Tris buffer pH 8.0: 17 ng mL^{-1} (1 nM) LOD; 1.7–1366 ng mL^{-1} (0.1–80 nM) LR In buffer/5% human serum: 17 ng mL^{-1} (1 nM) LOD; 17–3060 ng mL^{-1} (1–180 nM) LR LOD equation: 3σ rule	-NA
IFN-γ [126] (Lumin.; turn-on)	Ir(III) complex probe	-Dissociation of aptamer/G-rich-sequence duplex -G-quad formation	In Tris buffer pH 7.2: 2.04 ng mL^{-1} (0.12 nM) LOD; 17–1700 ng mL^{-1} (1–100 nM) LR LOD equation: 3σ rule	-NA
IFN-γ [56] (SPR; turn-on)	–	-Dissociation of aptamer/streptavidin duplex	In PBS pH 7.4: 0.51 ng mL^{-1} (0.03 nM) LOD; 5.1–5661 ng mL^{-1} (0.3–333 nM) LR In 10% healthy plasma (Parameter: NR) LOD equation: mean blank response + 3SD	-NA
IFN-γ [106] (FL; turn-on)	-Magnetic beads -LAMP -SYTO-9 dye	-Formation of DNA nanocomplex assembly and target recycling	In LAMP reaction mixture: 2.3 ng mL^{-1} LOD; 5–80 ng mL^{-1} LR In 10% serum: 92.8%–112.9% recovery LOD equation: (not specified)	-NA
IFN-γ [107] (PLM; turn-on)	DMOAP liquid crystal (LC)	-Change in orientation of LC	17 pg mL^{-1} (1 pM) LOD; 17–170 pg mL^{-1} (1–10 pM) LR. LOD equation (not specified) In clinical latent TB blood samples: (83% sensitivity due to matrix effect).	-Method of latent TB confirmation (not specified).
IFN-γ [108] (LSPR; turn-on)	AuNRDs labeled complementary DNA	-Indirect competition assay.	In PBS: 170 pg mL^{-1} (10 pM) LOD; 0.17–17 ng mL^{-1} (0.01–1 nM) LR In 10% FBS: (Parameters NR) LOD equation (not specified)	-NA
IFN-γ [109] (FL; turn-on)	-MNPs -CHA -FAM-liposome	-Change in aptamer hairpin structure	In PBS pH 7.4: 0.799 pg mL^{-1} (0.047 pM) LOD; 0.85 pg mL^{-1}–17 ng mL^{-1} (0.05–1000 pM) LR In human serum: 93.2–104.6% recovery LOD equation: S/N of 3	-NA
IFN-γ [110] (FL; turn-off)	-CuNPs reporter -SiNPs platform	-Change in aptamer hairpin structure	In buffer: 1 pg mL^{-1} LOD; 10 pg mL^{-1}–4 ng mL^{-1} LR. LOD equation: 3 × $SD_{blank}/slope_{calibration\ curve}$ In serum samples: 92.5%–98.3% recovery	-NA
IFN-γ [105] (CL; turn-on)	-Luminol-AuNPs platform	-Dissociation of aptamer/oligonucleotide duplex	In Tris buffer pH 7.4: 6.8 ng mL^{-1} (0.4 nM) LOD; 8.5–1700 ng mL^{-1} (0.5–100 nM) LR In Tris buffer/10% human serum (Parameters NR) LOD equation: S/N of 3	-NA
LAM [114] (Col.; turn-on)	-HRP reporter -Smartphone device	-Direct and Indirect dot-blot assay	In PBS: 10^4 CFU mL^{-1} (direct), 10^5 CFU mL^{-1} (indirect dot-blot assay) limit of quantification (LOQ); 10^4–10^7 CFU mL^{-1} LR In infected and healthy sputum samples (Parameters NR). LOQ equation (not specified)	-Acid fast staining -Culture method (Sensitivity of dot-blot assay comparable to culture method)
IFN-γ [104] (Col.; turn-on)	-DNAzyme -EXO III EATR	-Dissociation of aptamer/oligonucleotide duplex	In HEPES pH 7.4: 1.7 pg mL^{-1} (0.1 pM) LOD with UV–Vis., and 340 pg mL^{-1} (20 pM) LOD with the naked eyes. 34–340 pg mL^{-1} (2–200 pM) LR In 10% human serum: (Parameters NR) LOD equation: mean blank response + 3SD	-NA

The aptasensors listed above are reagentless.

For label-free FL aptasensors, fluorophores may be intercalated into the aptamer secondary structure, and changes in the FL intensities of the intercalated fluorophores may lead to increase or decrease in FL intensities on target binding. For instance, using intercalated thiazole orange (TO) FL reporter and a label-free G-quad IFN-γ aptamer structure formed in the presence of Na^+ and Mg^{2+}, Pan et al. (2013) fabricated a "turn-off" aptasensor with LOD of 2 nM [102]. Increase in FL was observed in the absence of IFN-γ but was decreased in the presence of IFN-γ due to structure switching of the G-quad aptamer structure and released TO. Similar assay strategy, but with the G-quad structure formed in the presence of thioflavin T (ThT) fluorescent probe, has been reported for a label-free IFN-γ aptasensor with LOD of 1 nM [103]. However, using a different assay format, a "signal-on" luminescence IFN-γ assay with LOD of 0.12 nM was reported based on interaction of a G-quad dsDNA with nascent iridium(III) complex. The G-quad dsDNA comprised of a label-free aptamer and G-quad DNA sequences, and interacted weakly with the Ir(III) complex in the absence of target. In the presence of IFN-γ, the G-quad structure was formed in the presence of K^+ due to the release of the G-quad DNA sequence on aptamer/target duplex formation. Emission intensity was increased by 6.0-fold due to the strong interaction of the luminescent Ir(III) complex and the G-quad structure [126].

Based on structure switching of IFN-γ/streptavidin bifunctional hairpin probe, immobilized on a Au/ZnO-based thin film chip substrate, a "signal-on" SPR IFN-γ aptasensor with 33 pM LOD has been reported. Switching of the bifunctional aptamer hairpin structure in the presence of target exposes the streptavidin sequence for streptavidin binding [56]. Detection was recorded as changes in SPR reflectivity due to the streptavidin binding. Also, a label-free "turn-on" IFN-γ FL aptasensor based on target-triggered DNA nanomachine self-assembly, coupled with loop-mediated isothermal amplification (LAMP) have been reported with 2.3 ng mL^{-1} LOD [106]. The formation of DNA nanomachine on target binding triggers target release and recycling, while LAMP technique increases FL signal of the intercalated SYTO-9 dye in real-time. In a different assay format, changes in liquid crystal (LC) orientation was monitored for a label-free LC-based IFN-γ aptasensor

[107]. This aptasensor with LOD of 1 p.m. (~17 pg mL^{-1}), was fabricated using (3-aminopropyl) triethoxysilane (APTES) and DMOAP (dimethyloctadecyl-[3-(trimethoxysilyl)propyl] ammonium chloride) LC-modified microscope glass slides for immobilization of label-free IFN-γ aptamer. Target binding induces changes in the LC orientation from homeotropic to random, and recorded as dark to light optical images using polarized light microscopy (PLM).

4.2.1. *Nanomaterial-assisted label-free optical aptasensors*

As sensing platforms and fluorophore labels, nanomaterials enhance optical performance of label-free aptasensors. In one instance, a localized surface plasmon resonance (LSPR) IFN-γ aptasensor with LOD of 10 pM based on indirect competition assay was reported using gold nanodot sensing platform and gold nanorods (AuNRDs)-functionalized complementary DNA as reporter molecule [108]. Changes in spectra shift and "turn-on" biosensing was recorded in the presence of IFN-γ due to release of AuNRDs-DNA. Likewise, a label-free "turn-on" FL IFN-γ aptasensor with LOD of 0.047 pM was recently reported based on magnetic nanoparticles (MNPs) sensing platform, target-responsive liposome and target induced catalytic hairpin assembly (CHA) [109]. The MNPs also served to eliminate interference due to unreacted peptide probe and liposome. Conformational change in the recognition probe (HP1) structure in the presence of IFN-γ led to exposure of the HP1 stem for hybridization with a complementary oligonucleotide (HP2), initiating target release and recycle for CHA. Target detection was achieved by the interaction of the FAM-encapsulated-liposome with an azido-labeled peptide probe capable of destroying liposome, causing leakage of FAM in the presence of MNPs. In another study, a "turn-off" IFN-γ aptasensor with LOD of 1 pg mL^{-1} was reported with streptavidin-coated silicon nanoparticles (SNPs-streptavidin) for immobilization of label-free aptamer hairpin, and copper nanoparticles (CuNPs) reporter (Fig. 8A) [110]. In this work, high FL intensity was reported in the absence of IFN-γ and ascorbic acid due to in-situ generation of CuNPs at the stem region of the aptamer hairpin. IFN-γ binding led to decrease in FL intensity due to switching of the aptamer hairpin structure and resulting inability to generate CuNPs *in situ*.

4.2.2. *Enzyme-based label-free optical TB aptasensors*

Typical examples of enzyme-based signal amplification strategies for label-free optical TB aptasensors include the use of enzyme-based

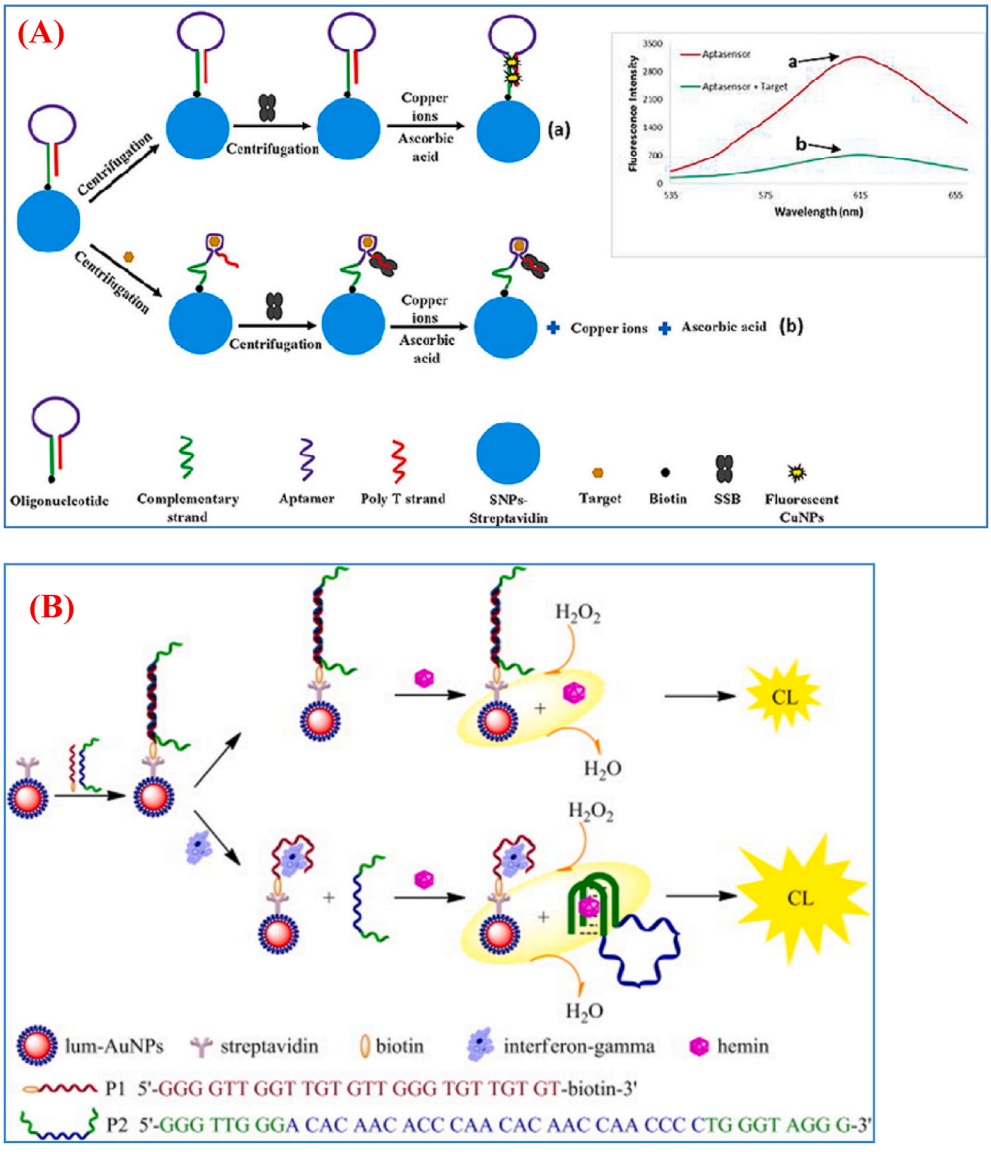

Fig. 8. Schematic illustration of (A) IFN-γ fluorescent aptasensor based on *in situ* generation of CuNPs [110], Copyright permission (2017) Elsevier, (B) A homogeneous hemin/G-quadruplex DNAzyme based turn-on CL IFN-γ aptasensor. detection via in-situ assembly of luminol-AuNPs, deoxyribonucleic acid, IFN-γ and hemin [105], Copyright permission (2013) Elsevier.

reporter molecules such as G-quad DNAzyme, HRP, and endo-/exo-nuclease for target recycling. Enzyme-based target recycling may be accompanied with nanomaterial sensing platforms for enhanced performance. For instance, a label-free "turn-on" chemiluminescence (CL) IFN-γ aptasensor with LOD of 0.4 nM was reported using luminol-AuNPs sensing platform and peroxidase-mimicking G-quad DNAzyme reporter probe (Fig. 8B) [105]. A biotinylated–IFN–γ-aptamer was first hybridized to 2-halves of a G-rich complementary oligonucleotide, and immobilized on streptavidin-modified luminol-AuNPs through biotin-streptavidin interaction. In the presence of IFN-γ, the dsDNA was dissociated, releasing the 2-halves of the G-rich complementary oligonucleotide which combined together to form a peroxidase-mimicking G-quad DNAzyme in the presence of hemin. Similarly, a recent smartphone-based direct and indirect dot-blot assay was fabricated using label-free aptamer, and HRP as a reporter molecule for ManLAM MTB biomarker [114]. The direct blot assay involved the use of nitrocellulose membrane sensing platform for immobilizing a label-free biotinylated aptamer conjugated to a streptavidin-labeled HRP, while the indirect dot-blot aptasensor was fabricated using a polyester cloth sensing platform for immobilizing the aptamer by UV irradiation. In both cases, the catalytic oxidation of 3,3′,5,5′-tetramethylbenzidine (TMB) by HRP, in the presence of H_2O_2 generated color changes which were monitored with the naked eyes or captured using smartphone or scanner. DNAzyme reporter molecule in combination with EXO III EATR amplification strategy was reported for another label-free "turn-on" colorimetric IFN-γ aptasensor. The aptasensor comprises a G-rich aptamer partially hybridized to a hybrid DNA1-DNA2 duplex, generating a 3′ protruding terminal. In the presence of IFN-γ, formation of aptamer/target duplex on release of aptamer from the DNA1-DNA2/aptamer complex, switches the 3′-protruding termini to a blunt-termini. This initiates digestion of aptamer and part of DNA1 by EXO III, and target release from the aptamer/target duplex, generating cycles of EATR amplification. In the presence of hemin, the released aptamer formed a G-quad structure which catalyzed the oxidation of colorless $ABTS^{2-}$ to green $ABTS^{(\cdot-)}$ in the presence of H_2O_2 [104].

5. Microfluidic-based TB aptasensors

Microfluidic devices (MFDs) are devices capable of processing small sample volumes using channels in the dimensions of ten to hundred micrometers. MFDs have found various applications in biosensing and biotechnology due to their numerous advantages such as cheaper and faster means of biosensing with small sample volumes, high resolution and sensitivity [127]. They are also idea for miniaturization, automation, multiplexing and POC applications. MFDs are developed by injection moulding, soft lithography, etching or 3-D printing techniques using silicon, glass, poly(dimethyl siloxane) (PDMS), thermoplastic, and paper as substrates. Integration of micropatterned electrode arrays to MFDs allow for design of microfluidic system with well-organized sites for cell capture and sensing element. MFDs-based aptasensors reported for TB biomarkers are summarized in Table 7. In one instance, a "signal-off" microelectrode array-based PDMS-MFDs with LOD of <60 pM, was reported for real-time monitoring of cytokine (IFN-γ) release from human CD4 T cells based on structure switching of a MB-labeled-aptamer hairpin [61]. The PDMS-MFDs consists of Au multi-electrode micropatterned by etching eight circular Au microelectrodes (300 μm each) on a Cr/Au coated glass slide, a poly(ethylene glycol) (PEG) layer for physisorption of antibodies and for definition of sites for cell attachment and sensing surface, and a 3-acryloxypropyltrichlorosilane protective layer to enhance adhesion of the PEG layer. T cell-specific antibodies were incubated on the PEG layer for capturing of CD4 T cells at close proximity to the electrode sensing surface. Release of IFN-γ from the captured T cells was triggered by mitogenic activation, and monitored by changes in electrochemical signal resulting from displacement of the MB probe on aptamer/target binding. From this study, rate of production and release of cytokine from the activated CD4

Table 7
TB Aptasensors Based on Microfluidic devices.

Target	Sensing surface; immobilization	Class of microfluidic system (MFS)	Assay format	Analytical parameters* (Linear range (LR); detection Limit (LOD); specificity, recovery rate) in pristine electrolyte and real sample	Comparison with standard techniques
IFN-γ [61] (SWV; turn-off)	Au micro array/3′ thiol; SAM −5′ MB label	-Au microelectrode array -PDMS MFD (Array-based MFS)	-Switching of aptamer hairpin	In RPMI buffer: < 1.02 ng mL^{-1} (<60 pM) LOD; 1.02–153 ng mL^{-1} (60 pM - 9 nM) LR; In primary T cells from red blood cells- depleted blood in RPMI/10% serum: 0.0079 pg $cell^{-1}$ h^{-1} rate LOD equation: 3 × SD	-NA
IFN- γ TNF-α [64] (SWV; turn-off)	Au microarray/5′ thiol; SAM 5′-MB-TNF-α and 5′-AQ-IFNγ label	-Au microelectrode array -PDMS MFD (Array-based MFS)	-Switching of aptamer hairpin	In RPMI buffer: 6.35 ng mL^{-1} IFN-γ LOD; 9–130 ng mL^{-1} LR Primary T cells from healthy human blood and monocytic U937 cell line in RPMI/10% serum (parameter NR) LOD equation: S/N of 3	-NA
IFN-γ TNF-α [65] (SWV; turn-off)	Au microarray/3′ thiol; SAM −5′ MB label	-Au microelectrode array -PDMS MFD (Array-based MFS)	-Switching of aptamer hairpin	In PBS pH 7.4: 1.02 ng mL^{-1} (0.06 nM) IFN-γ LOD; >170 ng mL^{-1} (>10 nM) IFN-γ LR Rate in RPMI/10% serum: 0.0074 ± 0.0002 pg $cell^{-1}$ h^{-1} in primary T cells from red blood cells-depleted blood, 0.0030 ± 0.0001 pg $cell^{-1}$ h^{-1} in monocyte cell. LOD equation: S/N of 3	-NA
IFN-γ [100] (FL; turn-on)	Cell membrane/3′-Chol.; hydrophobic interaction 5′-ROX; 3′-TAO .	-Droplet encapsulated cell -PDMS MFD (Droplet-based MFS)	switching of aptamer hairpin	In DPBS buffer: 14.5 ng mL^{-1} (10 nM) LOD; 292.4 ng mL^{-1}– 9350 ng mL^{-1} (17.2 nM−550 nM) LR In PBMC sample (parameters NR) LOD equation (not specified)	-ELISA (confirm release of IFN-γ by T cells after 2 h)
IFN-γ [101] (FL; turn-on)	5′-FAM	-PDMS MFD (Aptamer beacon-based MFS)	Dissociation of aptamer/CP duplex	In PBS (parameters NR) LOD equation (not specified)	-NA
IFN-γ [111] (SPR; turn-on)	-Au-COC prism/3′ thiol; SAM -Label free	Bifunctional IFN-γ/streptavidin aptamer (Membrane-MFD)	Change in aptamer hairpin	In PBS pH 7.4: 170 ng mL^{-1} (10 pM) LOD; 0.17–1700 ng mL^{-1} (0.01–100 nM) LR In clinical TB infected plasma samples (parameters NR) LOD equation: S/N of 3	-Method of TB confirmation in infected plasma samples not specified. Sensitivity NR

All the aptasensors listed above are reagentless, with the exception of ref. [101,111].

T cells was determined (0.0079 pg cell^{-1} h^{-1}).

Multiplex applications of similar array-based microfluidic system have also been reported for simultaneous detection of IFN-γ and TNF-α using anti-CD4 and anti-CD14 Ab to capture T cells and monocyte U937, respectively. In one instance, thiolated anthraquinone (AQ)-labeled IFN-γ and MB-labeled TNF-α hairpin aptamers were immobilized on the micropatterned electrode array. Simultaneous production, release and detection of IFN-γ and TNF-α were triggered on infusion of CD4 T cells and U937 monocytic cells into the microfluidic device to achieve LOD of 6.35 ng mL^{-1} for IFN-γ and 5.46 ng mL^{-1} for TNF-α, respectively [64]. In a similar array-based microfluidic aptasensor for multiplex monitoring of IFN-γ and TNF-α based on structure switching hairpin aptamers, using MB label for both hairpin aptamers and eight sets of half-ring Au microelectrode array. Each aptamer was immobilized on different sets of the half-ring electrodes array. This "signal-off" multiplex aptasensor achieved LOD of 0.06 nM and 0.58 nM for IFN-γ and TNF-α, respectively, with rate of production of IFN-γ from T cells (0.0074±0.0002 pg cell^{-1} h^{-1}) and monocyte cells (0.0030±0.0001 pg cell^{-1} h^{-1}), and TNF-α from T cells (0.0100±0.001 pg cell^{-1} h^{-1}) and monocyte cells (0.0160 ±0.0003 pg cell^{-1} h^{-1}) determined [65].

For optical monitoring of cytokine production and release from a single cell, a simple, high throughput droplet-based microfluidic aptasensor (Fig. 9) was recently fabricated with LOD of 10 nM [100]. This system comprises of single aptamer-decorated T cells encapsulated in picolitre water-in-oil droplets, and PDMS-based microfluidic device. The cholesterol-linked 5′-ROX fluorophore and 3′-TAO quencher terminated aptamer hairpin was anchored on the cell walls of T cells the hydrophobic interaction between the cholesterol tail and the phospholipid layer of the cell walls. FRET-based FL quenching was observed in the absence of target due to the close proximity of the fluorescent probe to the quencher as a result of preservation of hairpin structure, but was recovered in the presence of target [100]. Likewise, immobilization of aptamer beacon on microfluidic device provided a continuous flow bead-based microfluidic reactor capable of performing multistage mixing routine for another "turn-on" FRET-based biosensing of TB [101]. This reported FRET-based IFN-γ aptasensor consists of a biotin-labeled aptamer beacon, constructed by hybridizing a biotinylated 6-carboxyfluorescein (6-FAM)-labeled aptamer to a black hole quencher−1 (BHQ−1)-labeled complementary oligonucleotide (CP), and immobilized on an avidin-coated dual-mode hydrodynamic microfluidic "rail--trap-and-rail" device. Membrane-based microfluidic systems offer simple, flexible, low-cost, robust and miniaturized fluid processing capabilities for POC applications. A membrane-based SPR microfluidic aptasensor for real-time measurement of IFN-γ was reported with 10 pM based on structure switching of bifunctional aptamer hairpin [111]. This MFDs consists of a Au-coated cyclic olefin copolymer prism for immobilization of a label-free IFN-γ/streptavidin bifunctional hairpin aptamer, and a microfluidic sample handling device comprising of a rayon paper-based transport membrane and absorbent pad.

6. Sample preparation for aptasensor real sample analysis

In order to ensure practical application of TB aptasensors in real sample analysis, TB aptasensors performances have been reported in wide range of real sample matrix as shown in Tables 3–7 These include diluted standard serum samples, and wide range of clinical samples such as human blood, red blood cell depleted whole blood, serum, urine, sputum, MTB culture, peripheral blood mononuclear cells (PBMCs), and cell lines including cytokine-producing cells (T cells and monocytes), T cell acute lymphoblastic leukemia cell lines (CCRF-CEM), BV2 cells, and human embryonic kidney (HEK) 293T cells. While already purified real sample matrix are commercially available, they can also be prepared in the laboratory from healthy and TB infected real samples. Analysis using TB infected samples must be carried out in a class II biological safety cabinet to avoid exposure to infectious bacilli while ensuring protection to personnel, products and the environment. Clinical serum samples are usually obtained as a supernatant of centrifugated blood. The serum samples are preserved in aliquots at −80 °C and used either with or without salmon sperm DNA, which serves to reduce background interference in the real sample matrix [58,82,91,92,110]. Treatment of sputum samples involves addition of NaOH, dispersion by vortex, dilution and mixing with buffers, centrifugation and washing of the sediment with buffers [93]. In another instance, sputum samples for CFP10 detection were simply treated with a solution of NaOH in isopropanol, followed by room temperature incubation after severe shock [90]. Red blood cell (RBC)-depleted whole blood is prepared by removing RBCs from whole human blood using erythrocyte lysis solution, followed by concentration via centrifugation, and resuspension in culture medium [61]. To study IFN-γ release from human blood cells, clinical blood samples can be obtained from fractionated human blood cells after centrifugation, and subsequently treated with TB antigen such as ESAT6 to stimulate IFN-γ release [107]. Likewise, from whole blood, PBMCs is isolated following a process of dilution with 0.9% NaCl, and density gradient centrifugation (using Ficoll-Paque or Lymphoprep solutions) [62,97], after which mononuclear cells can be removed and resuspended in culture medium. T- and B-lymphocytes are collected as floating cells from the culture media while monocytes usually adhere to the culture plastic overtime [65]. $CD4^+$ T cells are also isolated from purified PBMCs population through negative selection by magnetic beads using human $CD4^+$ T cell enrichment kit [62] or by $CD4^+$ T-cell capture using anti-CD4 Ab-modified glass [65]. T cells may be used directly or subsequently stimulated with mytogenic solution (a solution of phorbol 12-myristate 13- acetate, PMA, and ionomycin) to induce secretion and release of cytokines (IFN-γ and TNF-α) [60,62]. For cell viability studies and cell imaging, BV2 cells, HEK cells and CCRF-CEM cells are cultured in a humidified incubator with 5% CO_2 in a culture medium maintained at 37 °C [95,96,99]. Before cell imaging, the cell nuclei may be stained with Hoechst 33 342 dye in the cell culture incubator [95].

Results of real sample analysis show that most TB aptasensors have

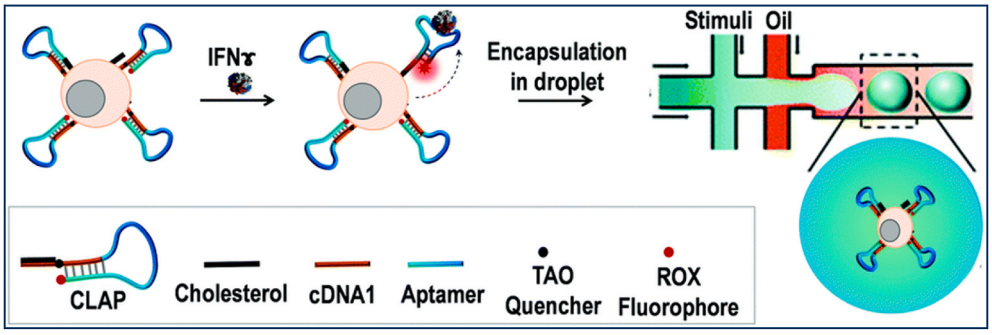

Fig. 9. Droplet-based microfluidic aptasensor schematic for probing IFN-γ secretion in single cells based on membrane-anchored fluorescence [100]. Reproduced under Creative Commons Attribution-NonCommercial 3.0 Unported License.

been able to recover above 90% of spiked concentrations of TB biomarkers in diluted standard serum, and overall sensitivity of 76.46%–95% and selectivity of 90%–100% in clinical samples. The recorded lower sensitivity in real samples is attributed to matrix effect due to background interference resulting from non-specific binding of serum or interaction with other biological components of the real sample matrix to the aptasensor. While ELISA technique was used in some cases to confirm IFN-γ production and release, and real-time bioimaging, comparatively, higher sensitivities were recorded with the aptasensors than ELISA. Likewise, though wide LR and appreciable LODs have been reported for several TB immunosensors [42,44], their lower temperature, pH and chemical stability, as well as the required sample pre-treatment steps might make immunosensors less ideal for POC application compared to aptasensors [85].

7. Conclusion and future perspective

Given the urgent need to eradicate TB globally, aptasensor-based TB detection is a step in the right direction. TB aptasensors offer great potential as POC diagnostic devices for early, cost-effective, simple, highly sensitive and specific diagnosis of TB. Factors such as transduction method, nature of aptamer sequence and signal amplification strategy contribute to the overall analytical performance of aptasensors. This review focuses on the sensitivities of recent TB aptasensors with respect to the aptamer sequence and modifications, assay formats, signal amplification strategies and analytical performances. Signal amplification is highly recommended for improved aptasensor performance as there is a remarkable relationship between the use of signal amplification strategy and the LR and LOD. Generally, wider LR and lower LOD were reported with signal amplification. For instance, LOD in "nano-" range (about 1.02–1.3 ng mL^{-1}) was recorded for MB-labeled IFN-γ electrochemical (ECM)-aptasensors without signal amplification, while "pico-" range (140 pg mL^{-1}) were recorded for MB-labeled IFN-γ ECM-aptasensors using a single amplification strategy (SiNWs). Likewise, for IFN-γ TB optical aptasensors, LOD in the "nano" range (2 pg mL^{-1}–6.76 ng mL^{-1}) were reported without nanomaterial and enzyme assisted amplification strategies, while LOD as low as 25.5 fg mL^{-1} was reported with several nanomaterials and enzymes. Similar trend was observed for label-free MPT64 ECM-aptasensors where LOD of 3.7 ng mL^{-1} was recorded with GDE, and 0.188 pg mL^{-1} with AuIDE electrode without additional amplification method, while improved LOD of 0.5 ±0.2 fg mL^{-1}–0.9 fg mL^{-1}, and 0.33 fg mL^{-1}–21 fg mL^{-1} were recorded with several nanomaterial-polymer composite amplification strategies for label-free and labeled MPT64 aptasensing, respectively. When compared with optical-based aptasensors, ECM-based TB aptasensors performed better with a wider linear range and better LOD. Few TB aptasensors performed contrary to the above range due to factors such as nature of aptamer sequence, type of aptamer label and detection strategy.

In terms of methodologies, label-free ECM aptasensors based on DPV detection technique show lower LOD (0.33 fg mL^{-1}–10 pg mL^{-1}) compared to SWV technique (0.14 ng mL^{-1}–2.2 ng mL^{-1}). Likewise, higher sensitivities were observed with sandwich assay format compared to structure switching aptamer hairpin assay format for the label-free ECM aptasensors. This may be due to the use of two high binding affinity aptamer molecules and a range of nanomaterials, fluorophore and enzyme as labels in sandwich assays. Also, SWV technique is recommended for label-free TB aptasensing rather than labeled TB aptasensor, as the former gave better LOD (2 fg mL^{-1}–19.38 pg mL^{-1}) compared to the latter with LOD within the range of 0.14 ng mL^{-1}–2.2 ng mL^{-1}. For the ECM TB aptasensor, though DPV and CV techniques show the lowest LOD, DPV is however recommended due to its higher sensitivity and greater peak resolution ability compared to CV. This might explain its very high frequency of use as a transduction method for the TB aptasensors reviewed (38.5% of all the ECM articles reviewed) compared to CV (7.7%). Likewise, FL technique is recommended for optical technique due to its high sensitivity to target. It is also the most frequently used technique for optical TB biomarker aptasensing, accounting for 59.1% of the optical techniques reviewed. The high sensitivity of these techniques notwithstanding, care must be taking in choosing the right transduction method as other factors such as nature of aptamer sequence, mode of assay format, and type and properties of the signal amplification methods, also contribute to aptasensor performance.

Despite the remarkable improvement in the performance of TB aptasensors, they are still far from being approved as a standard test for TB diagnosis. There is need to eliminate interference of other biological components of real samples to improve their clinical applications. Improvement of the individual limitations of each method would also translate to improvement in aptasensor performance. This includes improvement in surface homogeneity of ECM transducers, improvement in experimental reproducibility and reduction of undesirable transducer interference as well as label-to-probe interference in all techniques. There is also need for improvement in aptamer SELEX, with an increased understanding of the specific aptamer structure as it relates to target binding and possible interaction with other components of the aptasensor system. The use of nanomaterials as signal amplifiers call for improvement in nanomaterial synthesis with respect to size-control, enhanced properties, improved solubility and biocompatibility, and improved directional specificity of interaction. For translation of the aptasensor laboratory achievements obtained so far to POC devices, there is need for collaboration with industries and policy makers for early diagnosis of TB.

CRediT authorship contribution statement

Onyinyechi Vivian Uhuo: Conceptualization, Formal analysis, Visualization, Writing - original draft, Writing - review & editing. **Tesfaye Taddese Waryo:** Supervision. **Samantha Fiona Douman:** Conceptualization, Supervision, Writing - review & editing. **Kaylin Cleo Januarie:** Validation, and Writing-review and editing; **Kelechi Chiemezie Nwambaekwe:** Validation, and Writing-review and editing; **Miranda Mengwi Ndipingwi:** Validation, and Writing-review and editing; **Precious Ekwere:** Validation, and Writing-review and editing. **Emmanuel Iheanyichukwu Iwuoha:** Conceptualization, Supervision, Funding acquisition, Project administration.

Declaration of competing interest

The authors declare that they have no known competing financial interests or personal relationships that could have appeared to influence the work reported in this paper.

Data availability

No data was used for the research described in the article.

Acknowledgment

This work was funded by the National Research Foundation (NRF) of South Africa, Grant No. 85102, for the South African Research Chair Initiative (SARChI) Chair for NanoElectrochemistry and Sensor Technology.

References

[1] World Health Organization, Global Tuberculosis Report 2020, 2020. Geneva.
[2] World Health Organization, Global Tuberculosis Report 2021, 2021.
[3] R. Skolnik, Global Health 101 (Essential Public Health), 2011, p. 434.
[4] World Health Organization, Global Tuberculosis Report, 2017, 2017. https://doi.org/WHO/HTM/TB/2017.23.
[5] World Health Organization, Global Tuberculosis Report 2018, 2018. Geneva.
[6] World Health Organization, Global Tuberculosis Report 2019, 2019. Geneva.

[7] World Health Organization, Implementing Tuberculosis Diagnostics: A Policy Framework, 2015 https://doi.org/WHO/HTM/TB/2015.11.
[8] World Health Organization, The Use of Loop-Mediated Isothermal Amplification (TB-LAMP) for the Diagnosis of Pulmonary Tuberculosis, Policy Guidance, 2016.
[9] E. Lee, R.S. Holzman, Evolution and current use of the tuberculin test, Clin. Infect. Dis. 34 (3) (2002) 365–370, https://doi.org/10.1086/338149.
[10] F.A. Al-zamel, Detection and Diagnosis of Mycobacterium Tuberculosis, Expert Rev. Anti-infect. Ther. 7 (9) (2009) 1099–1108, https://doi.org/10.1586/eri.09.92.
[11] D. Goletti, E. Petruccioli, S.A. Joosten, T.H.M. Ottenhoff, Tuberculosis biomarkers: from diagnosis to protection, Infect. Dis. Rep. 8 (2) (2016) 24–32, https://doi.org/10.4081/idr.2016.6568.
[12] A.J. Atkinson, W.A. Colburn, V.G. DeGruttola, D.L. DeMets, G.J. Downing, D. F. Hoth, J.A. Oates, C.C. Peck, R.T. Schooley, B.A. Spilker, J. Woodcock, S. L. Zeger, Biomarkers and surrogate endpoints: preferred definitions and conceptual framework, Clin. Pharmacol. Ther. 69 (3) (2001) 89–95, https://doi.org/10.1067/mcp.2001.113989.
[13] V. Clifford, M. Tebruegge, C. Zufferey, S. Germano, J. Denholm, A. Street, E. McBryde, D. Eisen, N. Curtis, Serum IP-10 in the diagnosis of latent and active tuberculosis, J. Infect. 71 (6) (2015) 696–698, https://doi.org/10.1016/j.jinf.2015.08.001.
[14] D. Thierry, M.D. Cave, K.D. Eisenach, J.T. Crawford, J.H. Bates, B. Gicquel, J. L. Guesdon, IS6110, an IS-like element of Mycobacterium tuberculosis complex, Nucleic Acids Res. 18 (1) (1990) 188, https://doi.org/10.1093/nar/18.1.188.
[15] L. Bai, Y. Chen, X. Liu, J. Zhou, J. Cao, L. Hou, S. Guo, Ultrasensitive electrochemical detection of Mycobacterium tuberculosis IS6110 fragment using gold nanoparticles decorated fullerene nanoparticles/nitrogen-doped graphene nanosheet as signal tags, Anal. Chim. Acta 1080 (2019) 75–83, https://doi.org/10.1016/j.aca.2019.06.043.
[16] D.K. Turbawaty, A.K. Sugianli, A.Y. Soeroto, B. Setiabudiawan, I. Parwati, Comparison of the performance of urinary Mycobacterium tuberculosis antigens cocktail (ESAT6, CFP10, and MPT64) with culture and microscopy in pulmonary tuberculosis patients, Internet J. Microbiol. 2017 (2) (2017) 2–6, https://doi.org/10.1155/2017/3259329.
[17] K. Huygen, The immunodominant T-cell epitopes of the mycolyl-transferases of the antigen 85 complex of M. Tuberculosis, Front. Immunol. 5 (JUL) (2014) 1–11, https://doi.org/10.3389/fimmu.2014.00321.
[18] S.D. Shekhawat, H.J. Purohit, G.M. Taori, H.F. Daginawala, R.S. Kashyap, Evaluation of heat shock proteins for discriminating between latent tuberculosis infection and active tuberculosis: a preliminary report, J. Infect. Public Health 9 (2) (2016) 143–152, https://doi.org/10.1016/j.jiph.2015.07.003.
[19] Y.V.N. Cavalcanti, M.C.A. Brelaz, J.K.D.A.L. Neves, J.C. Ferraz, V.R.A. Pereira, Role of TNF-alpha, IFN-gamma, and IL-10 in the development of pulmonary tuberculosis, Pulm. Med. 1–10 (2012), https://doi.org/10.1155/2012/745483.
[20] H.A. Young, D.L. Hodge, Interferon-Gamma, Encyclopedia of Hormones, 2003, pp. 391–397.
[21] K. Schroder, P. Hertzog, T. Ravasi, D.A. Hume, Interferon-gamma : an overview of signals, mechanisms and functions, J. Leukoc. Biol. 75 (February) (2004) 163–189, https://doi.org/10.1189/jlb.0603252 (Journal).
[22] K. Law, M. Welden, T. Harkin, K. Tchou-wong, C. Chi, W.N. Rom, Tumor necrosis fador-a by bronchoalveolar cells lavaged from involved sites in pulmonary tuberculosis, Am. J. Respir. Crit. Care Med. 153 (1996) 799–804.
[23] C. Garbers, S. Heink, T. Korn, S. Rose-John, Interleukin-6: designing specific therapeutics for a complex cytokine, Nat. Rev. Drug Discov. 17 (6) (2018) 395–412, https://doi.org/10.1038/nrd.2018.45.
[24] L. Velazquez-Salinas, A. Verdugo-Rodriguez, L.L. Rodriguez, M.V. Borca, The role of interleukin 6 during viral infections, Front. Microbiol. 10 (MAY) (2019) 6–11, https://doi.org/10.3389/fmicb.2019.01057.
[25] M. Qi, J. Huang, H. Wei, C. Cao, S. Feng, Q. Guo, E.M. Goldys, R. Li, G. Liu, Graphene oxide thin film with dual function integrated into a nanosandwich device for in vivo monitoring of interleukin-6, ACS Appl. Mater. Interfaces 9 (48) (2017) 41659–41668, https://doi.org/10.1021/acsami.7b10753.
[26] T.A. Waldmann, The biology of interleukin-2 and interleukin-15: implications for cancer therapy and vaccine design, Nat. Rev. Immunol. 6 (8) (2006) 595–601, https://doi.org/10.1038/nri1901.
[27] T. Turgut, H. Akbulut, F. Deveci, C. Kacar, M.H. Muz, Serum interleukin-2 and neopterin levels as useful markers for treatment of active pulmonary tuberculosis, Tohoku J. Exp. Med. 209 (4) (2006) 321–328, https://doi.org/10.1620/tjem.209.321.
[28] R. Biselli, S. Mariotti, V. Sargentini, I. Sauzullo, M. Lastilla, F. Mengoni, V. Vanini, E. Girardi, D. Goletti, R. D'Amelio, R. Nisini, Detection of interleukin-2 in addition to interferon-γ discriminates active tuberculosis patients, latently infected individuals, and controls, Clin. Microbiol. Infect. 16 (8) (2010) 1282–1284, https://doi.org/10.1111/j.1469-0691.2009.03104.x.
[29] J.H. Dufour, M. Dziejman, M.T. Liu, J.H. Leung, T.E. Lane, A.D. Luster, T.E. Lane, A.D. Luster, IFN- γ -inducible protein 10 (IP-10; CXCL10)-deficient mice reveal a role for IP-10 in effector T cell generation and trafficking, J. Immunol. 168 (2002) 3195–32004, https://doi.org/10.4049/jimmunol.168.7.3195.
[30] D.R. Thévenot, K. Toth, R.A. Durst, G.S. Wilson, Electrochemical biosensors: recommended definitions and classification, Biosens. Bioelectron. 16 (1–2) (2001) 121–131, https://doi.org/10.1016/S0956-5663(01)00115-4.
[31] D. Moschou, L. Greathead, P. Pantelidis, P. Kelleher, H. Morgan, T. Prodromakis, Amperometric IFN-γ immunosensors with commercially fabricated PCB sensing electrodes, Biosens. Bioelectron. 86 (2016) 805–810, https://doi.org/10.1016/j.bios.2016.07.075.
[32] U.Z. Mohd Azmi, N.A. Yusof, J. Abdullah, S.A. Alang Ahmad, F.N. Mohd Faudzi, N.H. Ahmad Raston, S. Suraiya, P.S. Ong, D. Krishnan, N.K. Sahar, Portable electrochemical immunosensor for detection of Mycobacterium tuberculosis secreted protein CFP10-ESAT6 in clinical sputum samples, Microchim. Acta (2021), https://doi.org/10.1007/s00604-020-04669-x.
[33] H.J. Chung, C.M. Castro, H. Im, H. Lee, R. Weissleder, A magneto-DNA nanoparticle system for rapid detection and phenotyping of bacteria, Nat. Nanotechnol. 8 (5) (2013) 369–375, https://doi.org/10.1038/nnano.2013.70.
[34] M. Liong, A.N. Hoang, J. Chung, N. Gural, C.B. Ford, C. Min, R.R. Shah, R. Ahmad, M. Fernandez-Suarez, S.M. Fortune, M. Toner, H. Lee, R. Weissleder, Magnetic barcode assay for genetic detection of pathogens, Nat. Commun. 4 (2013) 1752–1759, https://doi.org/10.1038/ncomms2745.
[35] R. Khoder, H. Korri-Youssoufi, E-DNA biosensors of M. Tuberculosis based on nanostructured polypyrrole, Mater. Sci. Eng. C 108 (November 2019) (2020), 110371, https://doi.org/10.1016/j.msec.2019.110371.
[36] H. Šípová, V. Ševců, M. Kuchař, J.N. Ahmad, P. Mikulecký, R. Osička, P. Malý, J. Homola, Surface plasmon resonance biosensor based on engineered proteins for direct detection of interferon-gamma in diluted blood plasma, Sensor. Actuator. B Chem. 174 (2012) 306–311, https://doi.org/10.1016/j.snb.2012.08.024.
[37] S.T. Thanyani, V. Roberts, D.G.R. Siko, P. Vrey, J.A. Verschoor, A novel application of affinity biosensor technology to detect antibodies to mycolic acid in tuberculosis patients, J. Immunol. Methods 332 (1–2) (2008) 61–72, https://doi.org/10.1016/j.jim.2007.12.009.
[38] W. Liu, D. Zou, X. He, D. Ao, Y. Su, Z. Yang, S. Huang, Q. Zhao, Y. Tang, W. Ma, Y. Lu, J. Wang, X. Wang, L. Huang, Development and application of a rapid Mycobacterium tuberculosis detection technique using polymerase spiral reaction, Sci. Rep. 8 (1) (2018) 1–8, https://doi.org/10.1038/s41598-018-21376-z.
[39] H. Joshi, D. Kandari, S.S. Maitra, R. Bhatnagar, Biosensors for the detection of Mycobacterium tuberculosis: a comprehensive overview, Crit. Rev. Microbiol. (2022) 1–29, https://doi.org/10.1080/1040841X.2022.2035314.
[40] S.K. Rizi, E. Aryan, Z. Meshkat, G. Ranjbar, M. Sankian, K. Ghazvini, H. Farsiani, H.R. Pourianfar, M. Rezayi, The overview and perspectives of biosensors and Mycobacterium tuberculosis: a systematic review, J. Cell. Physiol. 236 (3) (2021) 1730–1750, https://doi.org/10.1002/jcp.30007.
[41] A. Rabti, A. Raouafi, N. Raouafi, DNA markers and nano-biosensing approaches for tuberculosis diagnosis, in: Nanotechnology Based Approaches for Tuberculosis Treatment, Elsevier Inc., 2020, pp. 207–230, https://doi.org/10.1016/B978-0-12-819811-7/00013-8.
[42] K.C. Januarie, O.V. Uhuo, E. Iwuoha, U. Feleni, Recent advances in the detection of interferon-gamma as a TB biomarker, Anal. Bioanal. Chem. 414 (2) (2022) 907–921, https://doi.org/10.1007/s00216-021-03702-z.
[43] M.R. Yerrapragada, D. Mampallil, Interferon- γ detection in point of care diagnostics: short review, Talanta 245 (2022), 123428, https://doi.org/10.1016/j.talanta.2022.123428.
[44] B. Golichenari, R. Nosrati, A. Farokhi-fard, M.F. Maleki, S. Mohammad, G. Hayat, K. Ghazvini, F. Vaziri, Electrochemical-based biosensors for detection of Mycobacterium tuberculosis and tuberculosis biomarkers tuberculosis and tuberculosis biomarkers, Crit. Rev. Biotechnol. 39 (8) (2019) 1057–1077, https://doi.org/10.1080/07388551.2019.1668348.
[45] B. Golichenari, K. Velonia, R. Nosrati, A. Nezami, A. Farokhi-Fard, K. Abnous, J. Behravan, A.M. Tsatsakis, Label-free nano-biosensing on the road to tuberculosis detection, Biosens. Bioelectron. 113 (2018) 124–135, https://doi.org/10.1016/j.bios.2018.04.059.
[46] K.L. Hong, L.J. Sooter, Single-stranded DNA aptamers against pathogens and toxins: identification and biosensing applications, BioMed Res. Int. 2015 (2015) 1–31, https://doi.org/10.1155/2015/419318.
[47] A. Dhiman, S. Haldar, S.K. Mishra, N. Sharma, A. Bansal, Y. Ahmad, A. Kumar, T. K. Sharma, J.S. Tyagi, Generation and application of DNA aptamers against HspX for accurate diagnosis of tuberculous meningitis, Tuberculosis 112 (July) (2018) 27–36, https://doi.org/10.1016/j.tube.2018.07.004.
[48] M. Darmostuk, S. Rimpelova, H. Gbelcova, T. Ruml, Current approaches in SELEX: an update to aptamer selection technology, Biotechnol. Adv. 33 (6) (2014) 1141–1161, https://doi.org/10.1016/j.biotechadv.2015.02.008.
[49] Z. Zhuo, Y. Yu, M. Wang, J. Li, Z. Zhang, J. Liu, X. Wu, A. Lu, G. Zhang, B. Zhang, Recent advances in SELEX technology and aptamer applications in biomedicine, Int. J. Mol. Sci. 18 (10) (2017) 1–19, https://doi.org/10.3390/ijms18102142.
[50] J.G. Bruno, J.L. Kiel, Use of magnetic beads in selection and detection of biotoxin aptamers by electrochemiluminescence and enzymatic methods, Biotechniques 32 (1) (2002) 178–183, https://doi.org/10.2144/02321dd04.
[51] R. Aimaiti, L. Qin, T. Cao, H. Yang, J. Wang, J. Lu, X. Huang, Z. Hu, Identification and application of SsDNA aptamers against H37Rv in the detection of Mycobacterium tuberculosis, Appl. Microbiol. Biotechnol. 99 (21) (2015) 9073–9083, https://doi.org/10.1007/s00253-015-6815-7.
[52] C.H. Weng, C.J. Huang, G. Bin Lee, Screening of aptamers on microfluidic systems for clinical applications, Sensors 12 (7) (2012) 9514–9529, https://doi.org/10.3390/s120709514.
[53] N. Tuleuova, C.N. Jones, J. Yan, E. Ramanculov, Y. Yokobayashi, A. Revzin, Development of an aptamer beacon for detection of interferon-gamma, Anal. Chem. 82 (5) (2010) 1851–1857, https://doi.org/10.1021/ac9025237.
[54] Y. Liu, N. Tuleouva, E. Ramanculov, A. Revzin, Aptamer-based electrochemical biosensor for interferon gamma detection, Anal. Chem. 82 (19) (2010) 8131–8136, https://doi.org/10.1021/ac101409t.
[55] L. Xu, S. Lei, Z. Liu, G. Ouyang, L. Zou, B. Ye, A label-free IFN-g aptasensor aptasensor based on target-triggered allosteric switching of aptamer beacon and

streptavidin-inorganic hybrid composites, Anal. Chim. Acta 1087 (2019) 29–35, https://doi.org/10.1016/j.aca.2019.08.034.
[56] C. Chang, S. Lin, C. Lee, T. Chuang, P. Hsueh, H. Lai, C. Lin, Amplified surface plasmon resonance immunosensor for interferon-gamma based on a streptavidin-incorporated aptamer, Biosens. Bioelectron. 37 (1) (2012) 68–74, https://doi.org/10.1016/j.bios.2012.04.038.
[57] C. Liu, G. Xiang, D. Jiang, L. Liu, F. Liu, F. Luo, X. Pu, An electrochemical aptasensor for detection of IFN-γ using graphene and a dual signal amplification strategy based on the exonuclease-mediated surface-initiated enzymatic polymerization, Analyst 140 (22) (2015) 7784–7791, https://doi.org/10.1039/C5AN01591J.
[58] K. Abnous, N.M. Danesh, M. Ramezani, M. Alibolandi, K.Y. Hassanabad, A. S. Emrani, A. Bahreyni, S.M. Taghdisi, A triple-helix molecular switch-based electrochemical aptasensor for interferon-gamma using a gold electrode and methylene blue as a redox probe, Microchim. Acta 184 (10) (2017) 4151–4157, https://doi.org/10.1007/s00604-017-2457-z.
[59] S.G. Meirinho, L.G. Dias, A.M. Peres, L.R. Rodrigues, Voltammetric aptasensors for protein disease biomarkers detection: a review, Biotechnol. Adv. 34 (5) (2016) 941–953, https://doi.org/10.1016/j.biotechadv.2016.05.006.
[60] B.P. Crulhas, D. Hadley, Y. Liu, D. Shin, G. Stybayeva, M. Imanbekova, A.E. Hill, V. Pedrosa, A. Revzin, An electrochemical aptasensor for detection of bovine interferon gamma, Anal. Methods 9 (31) (2017) 4527–4532, https://doi.org/10.1039/C7AY01313B.
[61] Y. Liu, J. Yan, M.C. Howland, T. Kwa, A. Revzin, Micropatterned aptasensors for continuous monitoring of cytokine release from human leukocytes, Anal. Chem. 83 (21) (2011) 8286–8292, https://doi.org/10.1021/ac202117g.
[62] Y. Liu, A. Rahimian, S. Krylyuk, T. Vu, B. Crulhas, G. Stybayeva, M. Imanbekova, D.S. Shin, A. Davydov, A. Revzin, Nanowire aptasensors for electrochemical detection of cell-secreted cytokines, ACS Sens. 2 (11) (2017) 1644–1652, https://doi.org/10.1021/acssensors.7b00486.
[63] Y. Chen, T.S. Pui, P. Kongsuphol, K.C. Tang, S.K. Arya, Aptamer-based array electrodes for quantitative interferon-γ detection, Biosens. Bioelectron. 53 (2014) 257–262, https://doi.org/10.1016/j.bios.2013.09.046.
[64] Y. Liu, T. Kwa, A. Revzin, Simultaneous detection of cell-secreted TNF-a and IFN-g using micropatterned aptamer-modified electrodes, Biomaterials 33 (2012) 7347–7355, https://doi.org/10.1016/j.biomaterials.2012.06.089.
[65] Y. Liu, Y. Liu, Z. Matharu, A. Rahimian, A. Revzin, Detecting multiple cell-secreted cytokines from the same aptamer-functionalized electrode, Biosens. Bioelectron. 64 (2015) 43–50, https://doi.org/10.1016/j.bios.2014.08.034.
[66] J. Xia, D. Song, Z. Wang, F. Zhang, M. Yang, R. Gui, L. Xia, S. Bi, Y. Xia, Y. Li, L. Xia, Single electrode biosensor for simultaneous determination of interferon gamma and lysozyme, Biosens. Bioelectron. 68 (2015) 55–61, https://doi.org/10.1016/j.bios.2014.12.045.
[67] K. Min, M. Cho, S. Han, Y. Shim, J. Ku, C. Ban, A simple and direct electrochemical detection of interferon-gamma using its RNA and DNA aptamers, Biosens. Bioelectron. 23 (2008) 1819–1824, https://doi.org/10.1016/j.bios.2008.02.021.
[68] S. Ding, C. Mosher, X.Y. Lee, S.R. Das, A.A. Cargill, X. Tang, B. Chen, E. S. McLamore, C. Gomes, J.M. Hostetter, J.C. Claussen, Rapid and label-free detection of interferon gamma via an electrochemical aptasensor comprising a ternary surface monolayer on a gold interdigitated electrode array, ACS Sens. 2 (2) (2017) 210–217, https://doi.org/10.1021/acssensors.6b00581.
[69] Y. Cao, W. Chen, P. Han, Z. Wang, G. Li, Target-driven self-assembly of stacking deoxyribonucleic acids for highly sensitive assay of proteins, Anal. Chim. Acta 890 (2015) 1–6, https://doi.org/10.1016/j.aca.2015.05.023.
[70] X. Miao, C.N. Ko, K. Vellaisamy, Z. Li, G. Yang, C.H. Leung, D.L. Ma, A cyclometalated iridium(III) complex used as a conductor for the electrochemical sensing of IFN-γ, Sci. Rep. 7 (2017), 42740 https://doi.org/10.1038/srep42740.
[71] H. Jin, R. Gui, X. Gao, Y. Sun, An amplified label-free electrochemical aptasensor of γ-interferon based on target-induced DNA strand transform of hairpin-to-linear conformation enabling simultaneous capture of redox probe and target, Biosens. Bioelectron. 145 (2019), 111732, https://doi.org/10.1016/j.bios.2019.111732.
[72] S. Farid, X. Meshik, M. Choi, S. Mukherjee, Y. Lan, D. Parikh, S. Poduri, U. Baterdene, C.E. Huang, Y. Yu, P. Burke, M. Dutta, M.A. Stroscio, Y.Y. Wang, P. Burke, M. Dutta, M.A. Stroscio, Detection of interferon gamma using graphene and aptamer based FET-like electrochemical biosensor, Biosens. Bioelectron. 71 (2015) 294–299, https://doi.org/10.1016/j.bios.2015.04.047.
[73] Y. Yin, L. Shi, Z. Chu, W. Jin, A highly sensitive electrochemical IFN-γ aptasensor based on a hierarchical graphene/AuNPs electrode interface with a dual enzyme-assisted amplification strategy, RSC Adv. 7 (71) (2017) 45053–45060, https://doi.org/10.1039/c7ra07817j.
[74] G. Yan, Y. Wang, X. He, K. Wang, J. Liu, Y. Du, A highly sensitive label-free electrochemical aptasensor for interferon-gamma detection based on graphene controlled assembly and nuclease cleavage-assisted target recycling amplification, Biosens. Bioelectron. 44 (1) (2013) 57–63, https://doi.org/10.1016/j.bios.2013.01.010.
[75] H. Li, S. Song, M. Wen, T. Bao, Z. Wu, H. Xiong, X. Zhang, W. Wen, S. Wang, A novel label-free electrochemical impedance aptasensor for highly sensitive detection of human interferon-gamma based on target-induced exonuclease inhibition, Biosens. Bioelectron. 142 (2019), 111532, https://doi.org/10.1016/j.bios.2019.111532.
[76] J. Zhao, C. Chen, L. Zhang, J. Jiang, R. Yu, An electrochemical aptasensor based on hybridization chain reaction with enzyme-signal amplification for interferon-gamma detection, Biosens. Bioelectron. 36 (1) (2012) 129–134, https://doi.org/10.1016/j.bios.2012.04.013.
[77] H. Zhang, B. Jiang, Y. Xiang, Y. Chai, R. Yuan, Label-free and amplified electrochemical detection of cytokine based on hairpin aptamer and catalytic DNAzyme, Analyst 137 (4) (2012) 1020–1023, https://doi.org/10.1039/c2an15962g.
[78] S. Noh, J. Kim, C. Park, J. Min, T. Lee, Fabrication of an electrochemical biosensor composed of multifunctional DNA three-way junction on Au microgap electrode for interferon gamma detection in human serum, Biomedicines 9 (692) (2021) 1–10, https://doi.org/10.1039/d0an02135k.
[79] Y. Chen, X. Liu, S. Guo, J. Cao, J. Zhou, J. Zuo, L. Bai, A sandwich-type electrochemical aptasensor for Mycobacterium tuberculosis MPT64 antigen detection using C60NPs decorated N-CNTs/GO nanocomposite coupled with conductive PEI-functionalized metal-organic framework, Biomaterials 216 (2019), 119253, https://doi.org/10.1016/j.biomaterials.2019.119253.
[80] N. Li, X. Huang, D. Sun, Y. Zhong, Z. Chen, A sensitive and rapid electrochemical aptasensor based on Au@PB for selective detection of Mycobacterium tuberculosis antigen MPT64, J. Electrochem. Soc. 166 (8) (2019) B604–B609, https://doi.org/10.1149/2.0651908jes.
[81] N. Li, X. Huang, D. Sun, W. Yu, W. Tan, Z. Luo, Z. Chen, Dual-aptamer-based voltammetric biosensor for the Mycobacterium tuberculosis antigen MPT64 by using a gold electrode modified with a peroxidase loaded composite consisting of gold nanoparticles and a Zr(IV)/Terephthalate metal-organic framework, Microchim. Acta 185 (12) (2018), https://doi.org/10.1007/s00604-018-3081-2.
[82] L. Bai, Y. Chen, Y. Bai, Y. Chen, J. Zhou, A. Huang, Fullerene-doped polyaniline as new redox nanoprobe and catalyst in electrochemical aptasensor for ultrasensitive detection of Mycobacterium tuberculosis MPT64 antigen in human serum, Biomaterials 133 (2017) 11–19, https://doi.org/10.1016/j.biomaterials.2017.04.010.
[83] M. Sypabekova, P. Jolly, P. Estrela, D. Kanayeva, Electrochemical aptasensor using optimized surface Chemistry for the detection of Mycobacterium tuberculosis secreted protein MPT64 in human serum, Biosens. Bioelectron. 123 (2019) 141–151, https://doi.org/10.1016/j.bios.2018.07.053.
[84] M. Sypabekova, K. Dukenbayev, A. Tsepke, A. Akisheva, N. Oralbayev, D. Kanayeva, An aptasensor for the detection of Mycobacterium tuberculosis secreted immunogenic protein MPT64 in clinical samples towards tuberculosis detection, Sci. Rep. 9 (1) (2019) 1–11, https://doi.org/10.1038/s41598-019-52685-6.
[85] H. Thakur, N. Kaur, D. Sareen, N. Prabhakar, Electrochemical determination of M. Tuberculosis antigen based on poly(3,4-ethylenedioxythiophene) and functionalized carbon nanotubes hybrid platform, Talanta 171 (2017) 115–123, https://doi.org/10.1016/j.talanta.2017.04.063.
[86] H. Thakur, N. Kaur, P. Sabherwal, D. Sareen, N. Prabhakar, Aptamer based voltammetric biosensor for the detection of Mycobacterium tuberculosis antigen MPT64, Microchim. Acta 184 (7) (2017) 1915–1922, https://doi.org/10.1007/s00604-017-2174-7.
[87] R. Das, A. Dhiman, S.K. Mishra, S. Haldar, N. Sharma, A. Bansal, Y. Ahmad, A. Kumar, J.S. Tyagi, T.K. Sharma, Structural switching electrochemical DNA aptasensor for the rapid diagnosis of tuberculous meningitis, Int. J. Nanomed. 14 (2019) 2103–2113, https://doi.org/10.2147/IJN.S189127.
[88] F. He, Y. Xiong, J. Liu, F. Tong, D. Yan, Construction of Au-IDE/CFP10-ESAT6 aptamer/DNA-AuNPs MSPQC for rapid detection of Mycobacterium tuberculosis, Biosens. Bioelectron. 77 (2016) 799–804, https://doi.org/10.1016/j.bios.2015.10.054.
[89] U.Z.M. Azmi, N.A. Yusof, J. Abdullah, F. Mohammad, S.A.A. Ahmad, S. Suraiya, N.H.A. Raston, F.N.M. Faudzi, S.K. Khiste, H.A. Al-Lohedan, Aptasensor for the detection of Mycobacterium tuberculosis in sputum utilising CFP10-ESAT6 protein as a selective biomarker, Nanomaterials 11 (9) (2021) 1–14, https://doi.org/10.3390/nano11092446.
[90] J. Li, K. Hu, Z. Zhang, X. Teng, X. Zhang, Click DNA cycling in combination with gold nanoparticles loaded with quadruplex DNA motifs enable sensitive electrochemical quantitation of the tuberculosis-associated biomarker CFP-10 in sputum, Microchim. Acta 186 (662) (2019) 2–7, https://doi.org/10.1007/s00604-019-3780-3.
[91] L. Li, Y. Yuan, Y. Chen, P. Zhang, Y. Bai, L. Bai, Aptamer based voltammetric biosensor for Mycobacterium tuberculosis antigen ESAT-6 using a nanohybrid material composed of reduced graphene oxide and a metal-organic framework, Microchim. Acta 185 (8) (2018) 379, https://doi.org/10.1007/s00604-018-2884-5.
[92] J. Xie, Z. Mu, B. Yan, J. Wang, J. Zhou, L. Bai, An electrochemical aptasensor for Mycobacterium tuberculosis ESAT-6 antigen detection using bimetallic organic framework, Microchim. Acta 188 (11) (2021), https://doi.org/10.1007/s00604-021-05058-8.
[93] X.Q. Zhang, Y. Feng, Q.Q. Yao, F. He, Selection of a new Mycobacterium tuberculosis H37Rv aptamer and its application in the construction of a SWCNT/aptamer/Au-IDE MSPQC H37Rv sensor, Biosens. Bioelectron. 98 (2017) 261–266, https://doi.org/10.1016/j.bios.2017.05.043.
[94] R.A. Karaballi, A. Nel, S. Krishnan, J. Blackburn, C.L. Brosseau, Development of an electrochemical surface-enhanced Raman spectroscopy (EC-SERS) aptasensor for direct detection of DNA hybridization, Phys. Chem. Chem. Phys. 17 (33) (2015) 21356–21363, https://doi.org/10.1039/c4cp05077k.
[95] K. Ma, F. Zhang, N. Sayyadi, W. Chen, A.G. Anwer, A. Care, B. Xu, W. Tian, E. M. Goldys, G. Liu, Turn-on" fluorescent aptasensor based on AIEgen labeling for the localization of IFN-γ in live cells, ACS Sens. 3 (2) (2018) 320–326, https://doi.org/10.1021/acssensors.7b00720.
[96] A. Tsuchiya, S.N. Hashim, S. Ise, T. Furuhata, K. Kawai, R. Wakabayashi, M. Goto, N. Kamiya, S. Sando, BODIPY-labeled fluorescent aptamer sensors for turn-on

sensing of interferon-gamma and adenine compounds on cells, Anal. Sci. 32 (5) (2016) 543–547, https://doi.org/10.2116/analsci.32.543.
[97] G. Liu, K. Zhang, K. Ma, A. Care, M.R. Hutchinson, E.M. Goldys, Graphene quantum dot based "switch-on" nanosensors for intracellular cytokine monitoring, Nanoscale 9 (15) (2017) 4934–4943, https://doi.org/10.1039/c6nr09381g.
[98] K. Hu, J. Liu, J. Chen, Y. Huang, S. Zhao, J. Tian, G. Zhang, An amplified graphene oxide-based fluorescence aptasensor based on target-triggered aptamer hairpin switch and strand-displacement polymerization recycling for bioassays, Biosens. Bioelectron. 42 (1) (2013) 598–602, https://doi.org/10.1016/j.bios.2012.11.025.
[99] N. Dhenadhayalan, M.I. Sriram, K.C. Lin, Aptamer-based fluorogenic sensing of interferon-gamma probed with ReS2 and TiS2 nanosheets, Sensor. Actuator. B Chem. 258 (2018) 929–936, https://doi.org/10.1016/j.snb.2017.11.178.
[100] L. Qiu, F. Wimmers, J. Weiden, H.A. Heus, J. Tel, C.G. Figdor, A membrane-anchored aptamer sensor for probing IFNγ secretion by single cells, Chem. Commun. 53 (57) (2017) 8066–8069, https://doi.org/10.1039/c7cc03576d.
[101] R.D. Sochol, D. Corbett, S. Hesse, W.E.R. Krieger, K.T. Wolf, M. Kim, K. Iwai, S. Li, L.P. Lee, L. Lin, Dual-mode hydrodynamic railing and arraying of microparticles for multi-stage signal detection in continuous flow biochemical microprocessors, Lab Chip 14 (8) (2014) 1405–1409, https://doi.org/10.1039/c4lc00012a.
[102] L. Pan, Y. Huang, C. Wen, S. Zhao, Label-free fluorescence probe based on structure-switching aptamer for the detection of interferon gamma, Analyst 138 (22) (2013) 6811–6816, https://doi.org/10.1039/c3an01275a.
[103] Z. Wang, X. Liu, Y. Huang, Q. Fan, W. Huang, Rapid and Reusable Detection of Interferon-Gamma Based on Label-free Single-Stranded DNA and Thioflavin T, vol. 18, 2018, pp. 2313–2317, 6.
[104] K. Zhang, T. Ren, K. Wang, X. Zhu, H. Wu, M. Xie, Sensitive and selective amplified visual detection of cytokines based on exonuclease III-aided target recycling, Chem. Commun. 50 (87) (2014) 13342–13345, https://doi.org/10.1039/c4cc05701e.
[105] J. Jiang, Y. He, X. Yu, J. Zhao, H. Cui, A homogeneous hemin/G-quadruplex DNAzyme based turn-on chemiluminescence aptasensor for interferon-gamma detection via in-situ assembly of luminol functionalized gold nanoparticles, deoxyribonucleic acid, interferon-gamma and hemin, Anal. Chim. Acta 791 (2013) 60–64, https://doi.org/10.1016/j.aca.2013.06.048.
[106] W. Chen, X. Fang, X. Ye, H. Li, H. Cao, J. Kong, DNA nanomachine-assisted magnetic bead based target recycling and isothermal amplification for sensitive fluorescence determination of interferon-γ, Microchim. Acta 184 (12) (2017) 4869–4877, https://doi.org/10.1007/s00604-017-2511-x.
[107] H.J. Kim, C.H. Jang, Liquid crystal-based aptasensor for the detection of interferon-Γ and its application in the diagnosis of tuberculosis using human blood, Sensor. Actuator. B Chem. 282 (November 2018) (2019) 574–579, https://doi.org/10.1016/j.snb.2018.11.104.
[108] D.Z. Lin, P.C. Chuang, P.C. Liao, J.P. Chen, Y.F. Chen, Increasing the spectral shifts in LSPR biosensing using DNA-functionalized gold nanorods in a competitive assay format for the detection of interferon-γ, Biosens. Bioelectron. 81 (2016) 221–228, https://doi.org/10.1016/j.bios.2016.02.071.
[109] H. Cui, B. Bo, J. Ma, Y. Tang, J. Zhao, H. Xiao, A target-responsive liposome activated by catalytic hairpin assembly enables highly sensitive detection of tuberculosis-related cytokine, Chem. Commun. 54 (38) (2018) 4870–4873, https://doi.org/10.1039/C8CC01542B.
[110] S.M. Taghdisi, N.M. Danesh, M. Ramezani, R. Yazdian-Robati, K. Abnous, An amplified fluorescent aptasensor based on single-stranded DNA binding protein, copper and silica nanoparticles for sensitive detection of interferon-gamma, Anal. Chim. Acta 984 (2017) 162–167, https://doi.org/10.1016/j.aca.2017.06.032.
[111] T.L. Chuang, C.C. Chang, Y. Chu-Su, S.C. Wei, X.H. Zhao, P.R. Hsueh, C.W. Lin, Disposable surface plasmon resonance aptasensor with membrane-based sample handling design for quantitative interferon-gamma detection, Lab Chip 14 (16) (2014) 2968–2977, https://doi.org/10.1039/c4lc00249k.
[112] N. Ansari, K. Ghazvini, M. Ramezani, M. Shahdordizadeh, R. Yazdian-Robati, K. Abnous, S.M. Taghdisi, Selection of DNA aptamers against Mycobacterium tuberculosis Ag85A, and its application in a graphene oxide-based fluorometric assay, Microchim. Acta 185 (21) (2018) 1–8, https://doi.org/10.1007/s00604-017-2550-3.
[113] J. Jeon, J. Lee, J. So, J.B. Lee, H. Lee, Y. Chang, S. Shin, J. Jo, C. Ban, Homogeneous fluorescent aptasensor for active tuberculosis diagnosis by direct quantification of circulating TB7.7 based on aptamer beacon with graphene oxide, Sensor. Actuator. B Chem. 317 (October 2019) (2020), 128126, https://doi.org/10.1016/j.snb.2020.128126.
[114] L. Li, Z. Liu, H. Zhang, W. Yue, C.W. Li, C. Yi, A point-of-need enzyme linked aptamer assay for Mycobacterium tuberculosis detection using a smartphone, Sensor. Actuator. B Chem. 254 (2018) 337–346, https://doi.org/10.1016/j.snb.2017.07.074.
[115] H. Li, X. Wang, S. Wei, C. Zhao, X. Song, K. Xu, J. Li, B. Pang, J. Wang, Applications of hybridization chain reaction optical detection incorporating nanomaterials : a review, Anal. Chim. Acta 1190 (2021), 338930, https://doi.org/10.1016/j.aca.2021.338930.
[116] Y.V. Gerasimova, D.M. Kolpashchikov, Enzyme-assisted target recycling (EATR) for nucleic acid detection, Chem. Soc. Rev. 43 (17) (2014) 6405–6438, https://doi.org/10.1039/c4cs00083h.
[117] R&D System, Recombinant Human IFN - γ, 2019.
[118] Sigma-Aldrich, Product Information Human Interferon-Gamma, 2014.
[119] EnoGene, MPT64 Protein, 2019.
[120] E. Akbari, Z. Buntat, M. Nilashi, A. Afroozeh, Y. Farhang, A. Zeinalinezhad, ISVR modeling of an interferon gamma (IFN-γ) biosensor based on graphene, Anal. Methods 8 (39) (2016) 7217–7224, https://doi.org/10.1039/c6ay01225f.
[121] M.H. Yunus, N.A. Yusof, N.H.A. Raston, S.S.M. Noor, Y. Sulaiman, J. Abdullah, A novel amperometric aptamer-antibody sandwich assay for the detection of tuberculosis with diazonium electrografted enhanced modified electrode, IEEE Sensor. J. 21 (20) (2021) 22442–22449, https://doi.org/10.1109/JSEN.2021.3108778.
[122] M. Fan, G.F.S. Andrade, A.G. Brolo, A review on recent advances in the applications of surface-enhanced Raman scattering in analytical Chemistry, Anal. Chim. Acta 1097 (2020) 1–29, https://doi.org/10.1016/j.aca.2019.11.049.
[123] P. Prakrankamanant, Quartz crystal microbalance biosensors: prospects for point-of-care diagnostics, J. Med. Assoc. Thail. 97 (SUPPL. 4) (2014) S56–S63.
[124] H. Huang, S. Shi, X. Gao, R. Gao, Y. Zhu, X. Wu, R. Zang, T. Yao, A universal label-free fluorescent aptasensor based on Ru complex and quantum dots for adenosine, dopamine and 17β-estradiol detection, Biosens. Bioelectron. 79 (2016) 198–204, https://doi.org/10.1016/j.bios.2015.12.024.
[125] M. Sharafeldin, J.J. Davis, Characterising the biosensing interface, Anal. Chim. Acta (2022), 339759, https://doi.org/10.1016/j.aca.2022.339759.
[126] S. Lin, B. He, C. Yang, C.H. Leung, J.L. Mergny, D.L. Ma, Luminescence switch-on assay of interferon-gamma using a G-quadruplex-selective iridium(III) complex, Chem. Commun. 51 (89) (2015) 16033–16036, https://doi.org/10.1039/c5cc06655g.
[127] A. Basiri, A. Heidari, M.F. Nadi, M.T.P. Fallahy, S.S. Nezamabadi, M. Sedighi, A. Saghazadeh, N. Rezaei, Microfluidic devices for detection of RNA viruses, Rev. Med. Virol. 31 (1) (2021) 1–11, https://doi.org/10.1002/rmv.2154.

Onyinyechi Vivian Uhuo is a doctoral student of the Department of Chemistry, University of the Western Cape, South Africa. She obtained her BSc in Industrial Chemistry from Ebonyi State University Nigeria, and her MSc in Physical Chemistry from University of Ibadan Nigeria, in 2011 and 2014, respectively. Currently, she is a Lecturer in the Department of Chemistry, University of Ibadan, Nigeria. Her research interests include nanomaterials synthesis and characterization, biosensor fabrication and application, and structure-function relationship of haemoglobin protein based on its sulphydryl reactivities.

Dr Tesfaye Waryo received his BSc (1992) and MSc (1996) in Chemistry fromAddis Ababa University (Ethiopia) and his PhD in Chemistry(2006) from the K.F. University of Graz (Austria). After briefly returning to Haramaya University (Alemaya, Ethiopia), he moved to South Africa in late 2006 to join Professor E.Iwuoha's research group (SensorLab) at the Department of Chemistry - University of the Western Cape, where Dr Waryo is currently a Senior Researcher (Electrochemical and Sensor Technology).With about 43 publications so far, his research encompasses molecularly functionalized bio-nanoelectrodic/ionodic systems for chemical sensor/biosensor, electrochromic/photovoltaicand battery/supercap applications.

Dr. Samantha Douman obtained her BSc and Ph.D in Chemistry from the University of the Western Cape and Dublin City University, respectively. She is currently with University of Cape Town, Department of Chemistry. Her research interest are largely directed towards developing ultrasensitive detection systems for diseases.

Kaylin Januarie is a PhD candidate at the Department of Chemistry, she obtained her BSc in Chemistry and her MSc in Nanoscience (Cum Laude) at the University of the Western Cape under the supervision of Professor Emmanuel Iwuoha. Her interests are in nanomaterials synthesis and the development of electrochemical biosensors for detection of diseases.

Kelechi C. Nwambaekwe is a PhD candidate at the University of the Western Cape Sensor Laboratories (SensorLab), where he obtained his MSc Chemistry degree (Cum Laude) in 2019. His doctoral research work focuses on the design, synthesis, characterization and photovoltaic application of inner transition metal-doped kesterite nanomaterials.

Miranda M. Ndipingwi obtained her BSc degree in Chemistry in 2011 at the University of Buea, Cameroon. She received her MSc in Nanoscience in 2016 and PhD in Physical Chemistry in 2020 at the University of the Western Cape (UWC), South Africa. She has been a postdoctoral researcher since 2020 at UWC under the guidance of her MSc and PhD supervisor, Prof Emmanuel Iwuoha. She has 18 publications in accredited journals. Her main research interests are in nanomaterial synthesis and applicationin electrochemical energy storage devices such as batteries and supercapacitors.

Precious Ekwere is a PhD research candidate with sensor laboratory, University of Cape Town, with part of her research work done at Universidad Autonoma de Madrid, Madrid, Spain. Her research interest is on the development of electrochemical energy storage materials and biosensors. She has co-authored publication in peer-review journals, and is a recipient of prestigious PhD scholarship/fellowship awards, including (i) the Junior Research Exchange Fellowship Award (2019) under the European Union H2020RISE INFINITE-CELL-DVL-777968 project; and (ii) the National Research Foundation (NRF) – The World Academy of Sciences (TWAS)/African Renaissance Doctoral Scholarship Award (2018–2021).

Emmanuel Iwuoha is a Professor of Chemistry; the South African (SA) Research Chair for NanoElectrochemistry and Sensor Technology; and the Founder and Director (since 2002) of the University of the Western Cape Sensor Laboratories (SensorLab) -a renowned centre of excellence for electrochemistry in Africa. His recent awards include: SA National Research Foundation (NRF) A-Rated Scientist Award 2019; NRF Champion of Research Capacity Development and Transformation Award 2020; and Honorary Fellow of the Royal Society of Chemistry (*HonFRSC*) UK Award 2021. He has over 360 publications, graduated 72 PhDs and given 36 Plenaries and 30 Keynotes. His editorial advisory board memberships include JACS Au, Analytical Chemistry and Bioelectrochemistry, among others.